iScience

CellPress
OPEN ACCESS

Article

Glucose oxidation-dependent survival of activated B cells provides a putative novel therapeutic target for lupus treatment

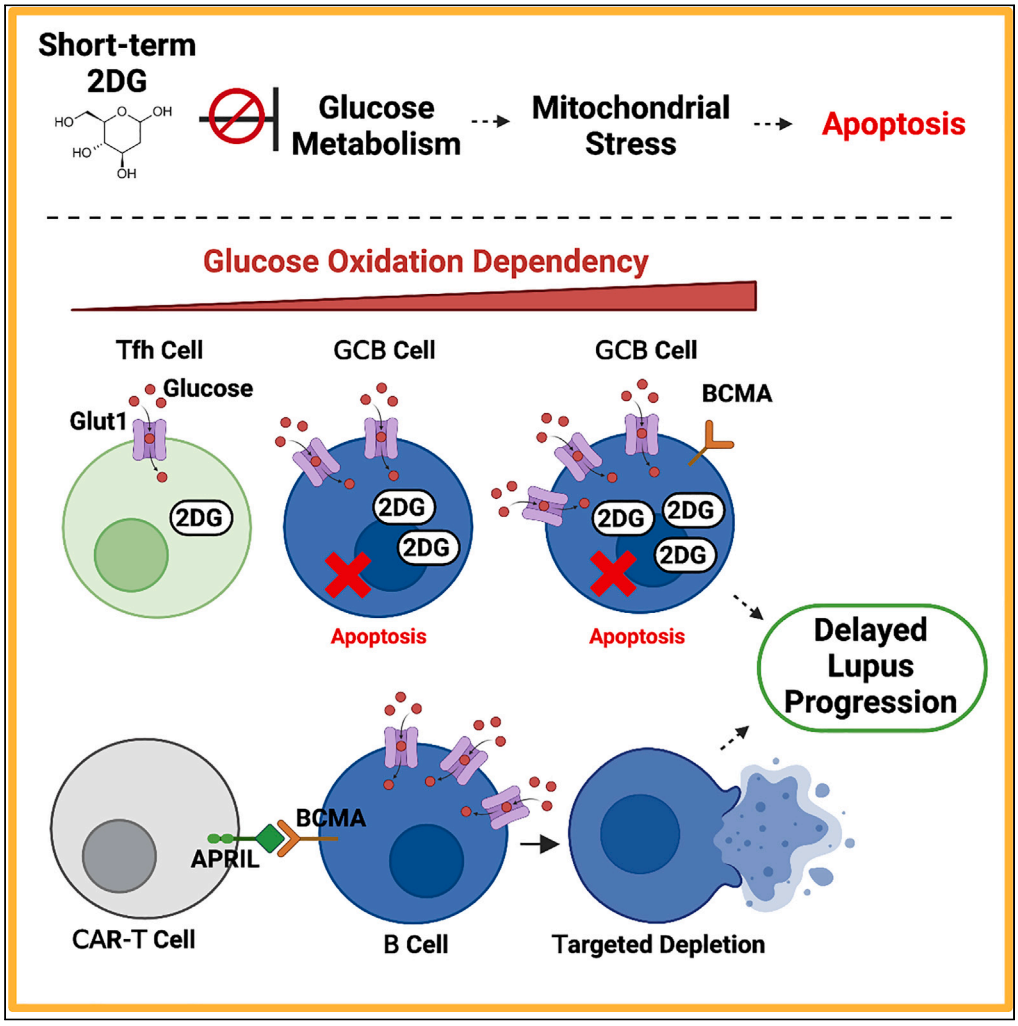

John J. Wilson, Jian Wei, Andrea R. Daamen, ..., Peter E. Lipsky, Derry C. Roopenian, Chih-Hao Chang

lucas.chang@jax.org

Highlights

Activated B and GCB cells in lupus heavily rely on glucose oxidation for survival

Short-term 2DG therapy selectively reduces activated B and GCB cells, easing lupus

Both lupus B and T cells show higher glycolytic demand than immunization

BCMA-targeted CAR-T cell treatment extends lupus mouse lifespan

Wilson et al., iScience 26, 107487
September 15, 2023
https://doi.org/10.1016/j.isci.2023.107487

iScience

CellPress
OPEN ACCESS

Article

Glucose oxidation-dependent survival of activated B cells provides a putative novel therapeutic target for lupus treatment

John J. Wilson,[1,7] Jian Wei,[1,2,7] Andrea R. Daamen,[3,7] John D. Sears,[1,4] Elaine Bechtel,[1] Colleen L. Mayberry,[1] Grace A. Stafford,[1] Lesley Bechtold,[1] Amrie C. Grammer,[3] Peter E. Lipsky,[3] Derry C. Roopenian,[1] and Chih-Hao Chang[1,5,6,8,*]

SUMMARY

Aberrant metabolic demand is observed in immune/inflammatory disorders, yet the role in pathogenesis remains unclear. Here, we discover that in lupus, activated B cells, including germinal center B (GCB) cells, have remarkably high glycolytic requirement for survival over T cell populations, as demonstrated by increased metabolic activity in lupus-activated B cells compared to immunization-induced cells. The augmented reliance on glucose oxidation makes GCB cells vulnerable to mitochondrial ROS-induced oxidative stress and apoptosis. Short-term glycolysis inhibition selectively reduces pathogenic activated B in lupus-prone mice, extending their lifespan, without affecting T follicular helper cells. Particularly, BCMA-expressing GCB cells rely heavily on glucose oxidation. Depleting BCMA-expressing activated B cells with APRIL-based CAR-T cells significantly prolongs the lifespan of mice with severe autoimmune disease. These results reveal that glycolysis-dependent activated B and GCB cells, especially those expressing BCMA, are potentially key lupus mediators, and could be targeted to improve disease outcomes.

INTRODUCTION

The autoimmune disease systemic lupus erythematosus (SLE, lupus) is characterized by loss of self-tolerance, leading to a dysregulated expansion of hyperactivated T and B cells.[1,2] Underlying lupus is the induction of T cell-dependent activation and clonal expansion of B cells in both germinal centers (GCs) and extrafollicular foci, resulting in their differentiation into plasma cells.[3,4] Increased expression of B cell maturation antigen (BCMA, or TNFRSF17) is observed on lupus B cells and is linked with increased activation via interactions with the cytokines TNFSF13 and 13B.[5,6] B cells, and particularly activated B cells, therefore present an attractive target for treatment of lupus, but to date only a few targeted treatments for this autoimmune disorder exist, including belimumab, a monoclonal antibody against TNFSF13B.[7,8]

$CD4^+$ T follicular helper (Tfh) cells are also critical drivers of lupus autoimmunity[9,10] by engaging follicular B cells in cognate and costimulatory interactions and secreting cytokines, especially interleukin (IL)-21, that promote germinal center B (GCB) cell proliferation and differentiation.[10–12] In turn, the expression of costimulatory molecules, such as ICOS-L and CD80/CD86 on activated B cells in the GC further promotes Tfh cell activation, differentiation, and Bcl6 expression.[13] Because of the co-dependency of Tfh and GCB cells, both are critical regulators of spontaneous GC formation during lupus.[1,9] A primary metabolic adaptation of activated lymphocytes is increased glucose metabolism,[14] likely mirrored in Tfh and activated B cells involved in lupus disease. This increased glucose metabolism can provide not only a rapid source of ATP but also glycolytic intermediates required for enhanced proliferation and effector function.[15,16] With this metabolic adaptation comes a potential avenue for therapeutic intervention by exploiting differential metabolic reliance between these activated cell types for precise treatment of disease. However, the metabolic requirements of discrete T and B cell populations in lupus are unclear, hindering the development of novel, targeted therapeutics.

Here, we examine the activation states and bioenergetics of activated B cells and circulating Tfh (cTfh) cells in the blood, and activated B cells, GCB cells, and Tfh cells in the spleen and lymph nodes, and elucidate

[1]The Jackson Laboratory, Bar Harbor, Maine, ME 04609, USA

[2]Department of Physiology and Pathophysiology, School of Basic Medical Sciences, Shandong University, Jinan, Shandong 250012, China

[3]AMPEL BioSolutions and the RILITE Research Institute, Charlottesville, VA 22902, USA

[4]Department of Microbiology and Immunology, University of North Carolina, Chapel Hill, NC 27599, USA

[5]Graduate School of Biomedical Sciences and Engineering, University of Maine, Orono, ME 04469, USA

[6]Graduate School of Biomedical Sciences, Tufts University School of Medicine, Boston, MA 02111, USA

[7]These authors contributed equally

[8]Lead contact

*Correspondence: lucas.chang@jax.org

https://doi.org/10.1016/j.isci.2023.107487

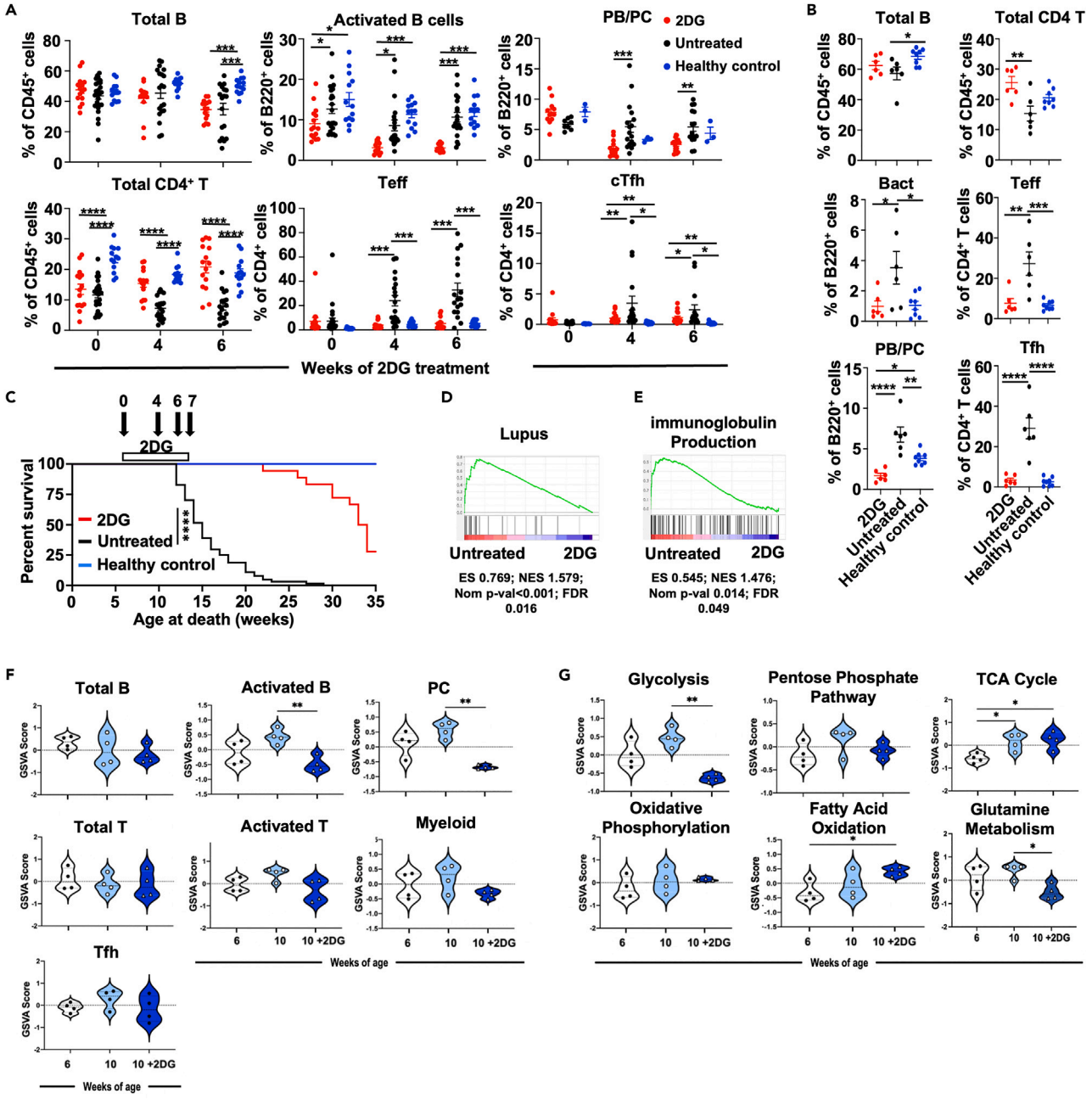

Figure 1. Glycolytic inhibition decreases disease biomarkers and increases life expectancy in lupus-prone mice

(A) Flow cytometry results of circulating lymphocytes of *Yaa* DKO mice treated with 2DG at 6-week-of-age for indicated weeks or untreated, and female DKO healthy controls (n = 15–25 mice per group).

(B) Flow cytometry results of splenic immune cells of 13-week-old *Yaa* DKO mice treated with 2DG for 7 weeks or untreated, or untreated female DKO healthy controls (n = 6–8 mice per group). Bact, activated B cells; PB/PC, plasmablasts/plasma cells.

(C) Survival of *Yaa* DKO mice treated with 2DG at 7-week-of-age, or untreated and female DKO healthy controls, with arrows showing sampling times (n = 15–25 mice per group). Data are from at least three independent experiments.

(D–G) GSEA plots of splenocytes from 10-week-old *Yaa* DKO mice untreated vs. treated with 2DG for 4 weeks (n = 4 mice per group). Enrichment of gene sets in (D) lupus and (E) immunoglobulin production. Violin plots of gene-expression data from splenocytes of individual 6-week-old (pre-symptomatic) untreated *Yaa* DKO mice (●), or 10-week-old *Yaa* DKO mice treated with 2DG (Symptomatic 2DG-treated) for 4 weeks (Δ) or untreated (Symptomatic) (○),

Figure 1. *Continued*

were analyzed by GSVA for enrichment of (F) immune cell and (G) metabolic pathway gene signatures. (n = 4 mice per group). Each dot represents one mouse. Error bars represent mean ± SEM; *p < 0.05, **p < 0.01, ***p < 0.001, ****p < 0.0001 using one-way ANOVA with Bonferroni's multiple comparison tests (A–B), Mantel-Cox test (C), or using Brown Forsythe and Welch's ANOVA with Dunnett's T3 multiple comparison tests (F–G). See also Figure S1 and Tables S2 and S3.

the effects of glycolytic inhibition on these populations. These data demonstrate that prolonged 2-deoxyglucose (2DG) treatment strongly affects the gene expression profile of activated B cells, particularly that of glycolysis activity; these cells are more highly correlated with the treatment and disease status than activated T cells. Moreover, we find that GCB cells, but not Tfh cells, exhibit markedly enhanced dependence on glucose oxidation via glycolysis, making them selectively susceptible to therapeutic intervention in spontaneous mouse models of lupus. Furthermore, one week of glycolytic inhibition (short-term) with 2DG preferentially induced elevated oxidative stress and apoptosis in both activated B and GCB cells, while leaving Tfh cells numerically and functionally unaffected. This numerical reduction of activated B and GCB cells correlated with significantly reduced mortality rates. We also found that a subset of GCB cells expressing BCMA exhibited markedly elevated glycolytic rates and a correspondingly increased sensitivity to short-term glycolytic inhibition. Reduction of $BCMA^+$ activated B cells with TNFSF13 (APRIL)-based CAR-T cells significantly delayed lupus progression, suggesting the importance of these cells in lupus pathogenesis. Overall, this work provides a pre-clinical proof-of-principle that short-term metabolic modulation via 2DG preferentially targets and reduces activated B and GCB cells, especially the BCMA-expressing subset. Moreover, this selective reduction is directly linked with reduced disease severity, revealing a potentially exploitable vulnerability to treat lupus, while minimizing broad-spectrum immunosuppression.

RESULTS

Long-term prophylactic glycolytic inhibition prevents severe autoimmunity

Long-term glycolytic inhibition via 2DG can attenuate development of cellular disease phenotypes in chronic lupus-prone mice.[17,18] We profiled immune cell populations over the course of disease progression in the acute lupus-prone mouse model, BXSB.Cg-*Cd8a*^{tm1Mak} *Il15*^{tm1Imx} *Yaa* (*Yaa* DKO),[19] and asked whether long-term glycolytic inhibition could result in increased lifespan. Six-week-old pre-symptomatic *Yaa* DKO mice showed decreased frequencies of circulating $CD4^+$ T cells when compared with healthy controls, but increased frequencies of cTfh cells, effector T (Teff), $CD25^+$ $CD4^+$ T cells, and myeloid cells (Figures 1A, S1A, and S1B). After 4 weeks of 2DG treatment (long-term), many of the cellular aberrations observed in untreated *Yaa* DKO mice (decreased $CD4^+$ T cell frequencies, increased Teff and cTfh-cell frequencies) were suppressed, whereas even after 6 weeks of treatment, frequencies of $CD25^+$ $CD4^+$ T cells, total B cells, and myeloid cells were unaffected. Moreover, the frequencies of $GL7^+$ activated B cells[20,21] in the peripheral blood were also reduced (Figures 1A and S1A). Flow cytometric analysis of spleen cells from untreated symptomatic *Yaa* DKO mice indicated expansion of Teff cells, Tfh cells, activated B cells, myeloid cells, plasmablasts/plasma cells, and $CD25^+$ $CD4^+$ T cells; 7 weeks of 2DG treatment reversed these abnormalities (Figures 1B and S1C). 2DG-treated mice exhibited greatly improved survival with the first fatality in the treated group occurring ~10 weeks after 2DG withdrawal, by which time 95% of untreated mice had died (Figure 1C). Overall, these results indicate that preventative glycolytic inhibition via 2DG is effective in ameliorating autoimmune activation and increasing survival in this model of severe lupus-like disease.

Long-term glycolytic inhibition potently affects B-lineage cells

Since the gene-expression patterns of T and B cells from lupus patients differ from those from healthy individuals,[22,23] we investigated whether 2DG treatment alters the dysregulated gene expression patterns in *Yaa* DKO spleens. We first conducted a principal component analysis (PCA) of differentially expressed genes to identify the major axes of variation in the data between pre-symptomatic, symptomatic, and symptomatic 2DG-treated mice (Figure S1D). We found that 2,238 genes were differentially expressed, 1,357 being upregulated and 881 downregulated with long-term 2DG treatment (Figure S1E). Gene ontology (GO) analysis revealed the downregulation of gene sets associated with endoplasmic reticulum (ER) stress, metabolism, and immune activation pathways with long-term 2DG treatment (Figure S1F). We further carried out Gene Set Enrichment Analysis (GSEA)[24,25] to compare gene-expression profiles of spleen cells from long-term 2DG-treated and -untreated *Yaa* DKO mice. Many genes dysregulated in human lupus were enriched in untreated mice, including those involved in immunoglobulin production (Figures 1D and 1E). To examine the effect of 2DG treatment in greater detail, we carried out Gene Set Variation Analysis (GSVA)[26,27] with a panel of curated gene modules and compared transcriptomic signatures in

spleens between 2DG-treated and -untreated symptomatic *Yaa* DKO mice at 10-week-of-age, and untreated pre-symptomatic mice at 6-week-of-age (Figure 1F). GSVA scores indicative of activated B cells and plasma cells were significantly decreased with 2DG treatment, whereas gene signatures of total T cells, total B cells, activated/effector T cells, Tfh cells, and myeloid cells were unaffected (Figure 1F). An analysis of metabolic pathways revealed that 2DG treatment decreased expression of genes controlling glycolysis and glutamine metabolism (Figure 1G). Linear regression analyses indicated a strong positive correlation between the glycolysis activity and cellular signatures for activated B cells and plasma cells, with positive, but weaker correlations for activated/effector T cells and myeloid cells (Figure S1G). Both activated B cells and plasma cells had strong positive correlations with glutamine metabolism, but less so than with glycolysis, whereas myeloid cells had a much weaker association. No cellular signatures were correlated with TCA cycle or oxidative phosphorylation (OXPHOS), whereas plasma cells had a negative correlation with fatty acid oxidation (FAO). Notably, although the activated/effector T cell gene signature was also influenced by prolonged 2DG, it was decreased to a much lesser degree. These data indicate that prolonged 2DG treatment strongly influences the metabolic regulation of activated B cell populations.

GCB cells show elevated glucose dependency compared to Tfh cells

Gene expression analysis suggested that activated B lineage cells appear to be more sensitive to long-term glycolytic inhibition than T cells. Given this disparity, we hypothesized that the metabolic requirements of activated B and Tfh cells might differ and, specifically, that activated B cells might have higher requirement for glycolysis. To test this, splenic-activated B and Tfh cells from symptomatic *Yaa* DKO mice were sorted (>95% purity, Figure S2A) to assess their bioenergetic profiles. Activated B cells were found to exhibit a greater bioenergetic profile, as evidenced by higher extra-cellular acidification rates (ECAR), an indicator of glycolysis, as well as higher oxygen consumption rates (OCR), an indicator of mitochondrial OXPHOS, compared to Tfh cells (Figure 2A). In contrast, both cell types had an equivalent glycolytic reserve (Figure S2B) indicating that the observed differences were not related to their ability to produce energy through glycolysis. Rather, the higher glucose consumption by activated B cells in *ex vivo* culture (Figure 2B) supports their greater utilization of glycolysis. To determine whether this elevated metabolic state was associated with disease, basal ECAR and OCR in activated B and Tfh cells from healthy, pre-symptomatic, and symptomatic *Yaa* DKO mice were assessed. We found that symptomatic mice displayed a significantly higher ECAR in both activated B and Tfh cells, whereas only activated B cells showed elevated OCR compared to pre-symptomatic or healthy mice (Figure 2C). Furthermore, this high bioenergetic profile of activated B cells was consistent in symptomatic NZBWF1 late-onset, chronic lupus-prone mice (Figure S2C), indicating that this may be a characteristic of activated B cells in murine lupus. Additionally, immune cells from symptomatic lupus-prone mice exhibited increased metabolic demand compared to immunized mice (Figures 2D and S2A), suggesting a potential link between metabolic reprogramming and lupus pathogenesis. Together, these data demonstrate that activated B cells exhibit a higher glucose usage and glycolysis rate than Tfh cells in lupus-prone mice, suggesting a potential link between metabolic activity and disease in these mice.

GCB cells are greatly expanded in mouse models of lupus.[1,18] Therefore, we measured the glucose uptake ability of $GL7^+$ $CD95^+$ GCB cells[20,28–30] isolated from 11-week-old symptomatic *Yaa* DKO mice. GCB cells showed greater expression of the major glucose transporter Glut1 (Figure 2E) and significantly higher 2-NBDG uptake than Tfh cells (Figure 2F). A comparison of glycolytic capacity indicated that Tfh cells can upregulate glycolysis rates in response to increased metabolic demand, while GCB cells have negligible glycolytic reserve (Figure 2G). To investigate whether enhanced glycolysis supports OXPHOS, we treated GCB and Tfh cells from symptomatic *Yaa* DKO mice with 2DG in the presence of glucose. Although 2DG reduced the basal ECAR of both GCB and Tfh cells to similar levels (Figure S2D), maximal respiratory capacity (MRC) was significantly decreased with 2DG treatment in GCB cells (27% reduction compared to untreated cells), but not in Tfh, non-GCB, or Teff cells (Figures 2H, 2I, and S2E), after FCCP-mediated mitochondrial decoupling, an indicator of OXPHOS reliance on a nutrient substrate fueling mitochondria.[31] A similar 2DG sensitivity (30% reduction compared to untreated cells) was also found in GCB cells from NZBWF1 mice (Figure S2F). These results suggest that the enhanced reliance on glycolysis in GCB cells from symptomatic lupus-prone mice supports OXPHOS.

To determine whether fueling the mitochondrial matrix in GCB cells from lupus-prone mice depends on glycolysis, we exposed cells to UK5099, which blocks the import of glycolysis-derived pyruvate into mitochondria for oxidation. Treatment with UK5099 significantly impaired the MRC of GCB cells (15% reduction

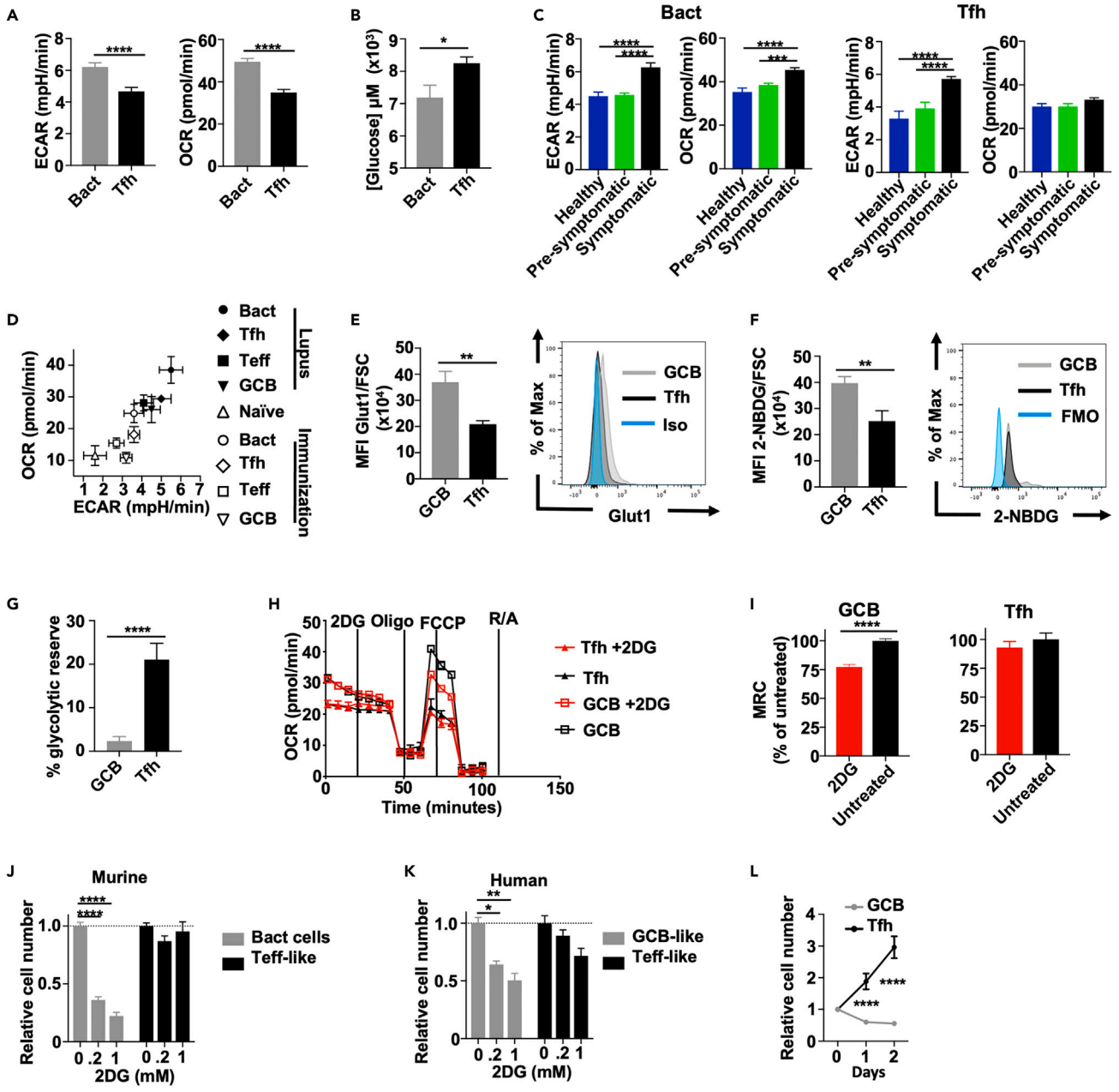

Figure 2. Activated B cells and GBC cells display augmented glycolytic dependency over Tfh cells

(A–J, L) Bioenergetic analysis of spleen cells from symptomatic *Yaa* DKO mice. (A) Basal ECAR and OCR of activated B cells (Bact) and Tfh cells. (B) Glucose concentration remaining after culture of Bact or Tfh cells in complete medium for 24 h, normalized to live-cell numbers. (C) Basal ECAR and OCR of Bact and Tfh cells from healthy, pre-symptomatic and symptomatic mice. (D) Basal OCR versus ECAR of *Yaa* DKO Bact (●), Tfh (◆), and Teff (■) GCB (▼) and immunization-induced Bact (○), Tfh (◇), Teff (□), GCB (▽), and naive (Δ) cells from C57BL/6 mice. (E) Glut1 expression on GCB and Tfh cells, mean fluorescence intensity (MFI) normalized to cell size (FSC). (n = 4–5 mice per group). (F) *In vivo* glucose uptake in GCB and Tfh cells measured as 2-NBDG MFI normalized to FSC (n = 4–5 mice per group). (G) Glycolytic reserve of GCB cells and Tfh cells. (H) OCR measurements of GCB and Tfh cells, with or without 2DG before treatment with oligomycin (Oligo), fluoro-carbonyl cyanide phenylhydrazone (FCCP), and rotenone/antimycin (R/A). (I) 2DG-effect on maximum respiratory capacity (MRC) was normalized to untreated cells and assessed as the contribution of glucose metabolism to OXPHOS (MRC % of untreated) in GCB and Tfh cells following FCCP exposure. Relative live-cell numbers of (J) murine Bact cells and Teff-like cells or (K) human GCB-like or Teff-like cells after 24-h treatment with 2DG, normalized to untreated controls. (L) Live GCB and Tfh cell-numbers in the presence of 1 mM 2DG, normalized to untreated controls. Data are from at least three independent samples. Error bars represent mean ± SEM; ns $p \geq 0.05$, *$p < 0.05$, **$p < 0.01$, ***$p < 0.001$, ****$p < 0.0001$ using unpaired two-tailed Student's *t*-tests (A–B, E–G, and I) or one-way ANOVA with Bonferroni's multiple comparison tests (C and J–L). See also Figure S2.

compared to untreated cells) but had no effect on Tfh cells (Figure S2G). We further evaluated whether mitochondrial fueling of GCB cells also depends on other catabolic pathways. We therefore treated GCB and Tfh cells with BPTES, a glutaminase inhibitor[32]; etomoxir, which suppresses mitochondrial FAO; or thioridazine, a selective inhibitor of peroxisomal FAO.[28] Treatment with BPTES resulted in a small, but significant, reduction of MRC (7.7% reduction compared to untreated cells) in GCB cells but not in Tfh cells (Figure S2H); however, this reduction was much less than that found with 2DG treatment (Figure 2I). Conversely, no change in MRC was observed in either GCB or Tfh cells treated with etomoxir or thioridazine (Figures S2I and S2J). Together, these results are consistent with the reliance of GCB cells on glucose as the primary anaplerotic precursor supporting mitochondrial function, whereas Tfh cells exhibit greater metabolic flexibility in mouse models of lupus.

Short-term inhibition of glucose oxidation selectively targets GL7$^+$ activated B and GCB cells but not cTfh or Tfh cells

Although early long-term 2DG treatment was effective at preventing disease in *Yaa* DKO mice, the effects of prolonged glycolytic inhibition might be too immunosuppressive for safe clinical application. Given their increased glycolytic dependency, we hypothesized that short-term inhibition of glucose oxidation with 2DG might selectively inhibit activated B and GCB cells. To test this, mouse splenocytes were activated *in vitro*. Numbers of differentiated GL7$^+$ activated B cells were significantly decreased by 2DG exposure, whereas CD44$^+$ Teff-like cells were not significantly affected (Figure 2J). A similar trend in 2DG sensitivity was found using *in vitro* activated human peripheral blood mononuclear cells (PBMCs) (Figure 2K). Glycolytic blockade with the hexokinase inhibitor 3-bromopyruvate also selectively decreased numbers of cultured murine-activated B cells (Figure S2K), further suggesting the efficacy of glycolytic inhibition. We next assessed the effect of 2DG treatment on the survival of splenic GCB and Tfh cells isolated from symptomatic *Yaa* DKO mice. One-day 2DG exposure significantly reduced GCB-cell numbers, which decreased further after two days, whereas expansion of Tfh cells was observed (Figure 2L). Next, we assessed circulating activated B and cTfh cells (Figure S3A) in symptomatic *Yaa* DKO mice as treatment progressed and found that activated B cell numbers dropped significantly by day 7 of therapy with no cTfh-cell reduction (Figure S3B). No other circulating populations, including plasmablasts/plasma cells, showed significantly reduced frequencies or numbers compared to untreated controls with this 1-week (short-term) treatment course (Figures 3A, S3A, and S3C). A similar reduction in frequencies and numbers of GCB cells was observed in both lymph nodes (Figures 3B and S3D) and spleens (Figures 3C and S3E) of treated mice, with no significant reductions in other populations in these organs. Numbers of splenic follicular regulatory T (Tfr), T regulatory (Treg), and transitional, follicular, marginal zone, and extrafollicular B cells were also unaffected following short-term treatment (Figures S4A–S4D). We also observed a comparable 2DG-induced reduction in frequency and cell numbers of GCB cells gated based on CD95^{hi} CD38^{low} GCB-cell markers[28] (Figure S4E). These data indicate that short-term inhibition of glucose oxidation with 2DG preferentially affects survival of activated B and GCB cells, while sparing Tfh cells.

To test whether this dual reduction of activated B and GCB cells can abrogate severe disease, we treated 11-week-old *Yaa* DKO mice with 2DG for 1 week and monitored their survival. The mean lifespan of untreated mice was 15.4 weeks, in contrast to 24.1 weeks for 2DG-treated mice (Figure 3D). Of note, the mice showed no significant decrease in frequencies of circulating Tfh or Teff cells after 2DG treatment removal (Figure S4F), suggesting that therapeutic efficacy was unlikely to be conveyed by a post-treatment reduction of these populations. Symptomatic NZBWF1 mice treated with short-term 2DG also displayed significant lifespan extension that correlated with a small reduction in circulating activated B cells and a significant decrease in splenic GCB cells (Figures S4G and S4H). Overall, the data suggest that increased sensitivity to the inhibition of glucose oxidation is a uniform feature of activated B and GCB cells from these diverse lupus-prone mouse models, rendering them comparatively more vulnerable than other cell types, suggesting that multiple lupus models can be positively impacted by short-term 2DG treatment.

To better understand the involvement of 2DG-responsive activated B and GCB cells in disease pathogenesis, an adoptive transfer approach was undertaken. We reduced the numbers of activated B and GCB cells in *Yaa* DKO mice by administering 2DG for one week (Figures 3A, 3B, and 3C) before transferring flow cytometry-sorted autologous activated B and GCB cells or GL7$^-$ B cells from symptomatic *Yaa* DKO mice. Mice that received activated B and GCB cells had significantly shorter mean lifespan (19.0 weeks) than those receiving GL7$^-$ B (23.8 weeks) or no cells (24.1 weeks) (Figure 3E). These data demonstrate that short-term 2DG treatment was remarkably effective in reversing disease trajectory with a concomitant

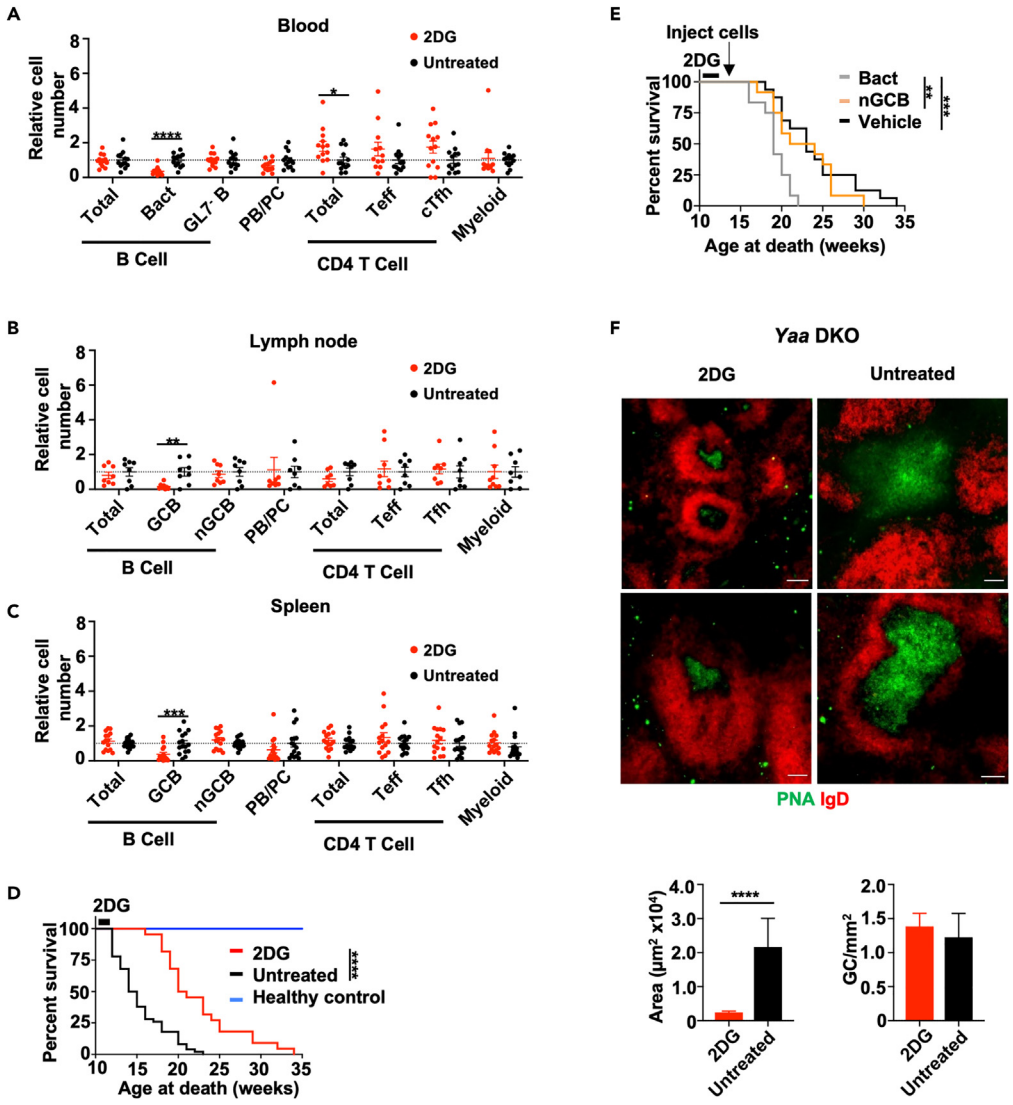

Figure 3. Short-term glycolytic inhibition selectively reduces activated B and GCB cells and improves survival outcomes

(A–C) Relative cell numbers from (A) peripheral blood, (B) lymph node, and (C) spleen normalized to untreated mice after 1 week of 2DG exposure in *Yaa* DKO mice (n = 13–15 mice per group). Relative cell numbers for 2DG treatment were generated by dividing cell numbers in individual 2DG-treated mice by the mean of all untreated controls.

(D) Survival of symptomatic *Yaa* DKO mice treated with 2DG for 1 week starting at 11-week-old, age-matched untreated mice, and female DKO healthy controls (n = 22–50 mice per group).

(E) Survival of 1-week 2DG-treated, symptomatic *Yaa* DKO mice followed by adoptive transfer of activated B cells (Bact), $GL7^-$ B cells, or vehicle control (n = 14 mice per group).

(F) Immunohistochemistry images of symptomatic *Yaa* DKO spleens from mice treated with 2DG for 1 week or untreated control mice were stained with anti-IgD (red) and anti-PNA (green) for germinal center identification. (Scale bars = 100 μm, n = 3). Data are from at least two independent experiments. Each dot represents one mouse. Error bars represent mean ± SEM; *p < 0.05, **p < 0.01, ***p < 0.001, ****p < 0.0001 using one-way ANOVA with Bonferroni's multiple comparison tests (A–C), Mantel-Cox tests (D-E), or using an unpaired two-tailed Student's *t* test (F). See also Figures S3 and S4.

decrease in mortality. We then examined the effect of short-term 2DG treatment on splenic morphology. Histologic examination of spleens showed that treatment of *Yaa* DKO mice with short-term 2DG significantly reduced the size, but not the number, of GCs (Figure 3F). In contrast, short-term 2DG treatment had no significant effect on splenic GC morphology in NZBWF1 mice (Figure S4I), consistent with the lower efficacy of 2DG in reducing GCB-cell numbers in these mice (Figures 3C and S4H). Taken together, our

results demonstrate that short-term inhibition of glucose oxidation with 2DG can effectively target and reduce the numbers of activated B and GCB cells, leading to a significant extension of lifespan in lupus-prone mice models. However, further optimization of 2DG treatment in NZBWF1 mice may be necessary to fully understand its potential benefits and compare them to those observed in *Yaa* DKO mice.

Glycolytic inhibition results in preferential induction of apoptosis of both activated B and GCB cells

Inhibition of glycolysis can cause cell death through apoptosis.[33] To determine how activated B and GCB cells are reduced, we treated symptomatic *Yaa* DKO mice with 2DG to assess cellular apoptosis. By day 4 of treatment, there was a significant increase in relative frequencies of pre-apoptotic (Annexin^{+}/PI^{-}) activated B cells, but not cTfh cells, in 2DG-treated mice (Figure 4A). With 2DG treatment, there was a trend toward increased apoptosis in activated B cells on day 7, but no such trend for cTfh cells (Figure 4A). Similarly, splenic GCB cells isolated from 7-day 2DG-treated mice showed increased pre-apoptosis (Figures 4B and S5A). In contrast, frequencies of pre-apoptosis were unchanged and apoptosis was significantly decreased in Tfh cells (Figure 4B). Moreover, 2DG treatment did not alter GL7 expression on activated B cells (Figure S5B), nor did it reduce numbers or frequencies of splenic GL7-expressing Teff in *Yaa* DKO mice (Figure S5C). Together, these data suggest that reductions in activated B and GCB cells after short-term 2DG exposure stem from selective reduction through apoptosis, not through loss of the GL7 surface marker.

Apoptosis can be induced by ER stress and the unfolded protein response (UPR).[33,34] The inositol-requiring enzyme 1/X-box-binding protein 1 (XBP1) pathway is a potent UPR signaling pathway in mammalian cells, promoting ER-induced apoptosis. To ascertain whether UPR signaling is elevated with short-term 2DG treatment, we assessed mRNA expression of *Xbp1* and its spliced form, *Xbp1s*, as markers of ER stress.[34,35] *Xbp1* expression in both GCB and Tfh cells from short-term 2DG-treated *Yaa* DKO mice were unchanged (Figure 4C), whereas expression of *Xbp1s* was decreased in Tfh cells with 2DG treatment, suggesting that neither GCB nor Tfh cells experienced ER stress *in situ* following transient 2DG treatment. Glucose deprivation may reduce cellular ATP production and increase reactive oxygen species (ROS) levels, leading to oxidative stress and the subsequent death of tumor cells.[36,37] Hence, we interrogated cells from *Yaa* DKO mice treated with short-term 2DG and found that the overall ATP production rate was reduced in GCB cells but not in Tfh cells, compared with those isolated from untreated mice (Figure 4D), which was corroborated with a reduction in total ATP (Figure 4E). We, therefore, examined the accumulation of mitochondrial ROS as an indicator of oxidative stress[37] in *Yaa* DKO mice. Following 2DG treatment, ROS production was significantly elevated in GCB cells, but was unchanged in Tfh cells (Figure 4F), non-GCB, and Teff cells (Figure S5D); whereas neither Tfh nor GCB cells experienced changes in mitochondrial mass (Figure S5E). Excessive ROS production in GCB cells was also linked to increased mitochondrial membrane potential (Figure S5F). Taken together, these data suggest that inhibition of glycolysis with 2DG selectively induces apoptosis of activated B and GCB cells, potentially through oxidative stress mediated by reduced ATP production and elevated mitochondrial ROS levels.

Short-term glycolytic inhibition targets hyperactive GCB cells while preserving functional integrity of Tfh and GCB cells

Tfh cells are vital to the formation and stability of GCs, as they provide survival and differentiation signals to GCB cells,[1,9] whereas IL-6, secreted by activated B cells, collaborates with IL-21 to induce Tfh cell differentiation and GC formation.[38,39] Tfh cell-derived IL-21 is thought to play a pivotal role in lupus pathogenesis and is the major cytokine inducing B-cell differentiation.[11,12,19] Although numbers of Tfh cells were unaffected by short-term glycolytic inhibition, it remained possible that 2DG treatment impaired Tfh-cell functionality and thus contributed to GCB cell apoptosis. To test this possible mechanism of reduction, splenic Tfh cells were isolated from *Yaa* DKO mice following 1-week 2DG treatment and examined for functional markers. Notably, neither the frequency of IL-21-producing Tfh cells nor IL-21 expression differed following treatment (Figure 5A). Likewise, the frequency of GCB cells producing IL-6 and the expression of this cytokine were both unaltered (Figure S6A). We found that Bcl6 protein expression, essential for the development of both Tfh and GCB cells,[40,41] was not impacted by 2DG in either Tfh or GCB cells (Figure 5B). In addition, the expression and frequency of Ki-67, a proliferation marker, in both Tfh and GCB cells were also unaffected by 2DG (Figure 5C). Furthermore, no treatment-induced reduction in the frequency or expression of the GCB-Tfh-cell interaction molecules ICOS-L, CD40, CD80, or CD86 on GCB cells (Figure S6B), nor ICOS, CD40L or CD28 on Tfh cells was observed (Figure S6C). We further examined whether

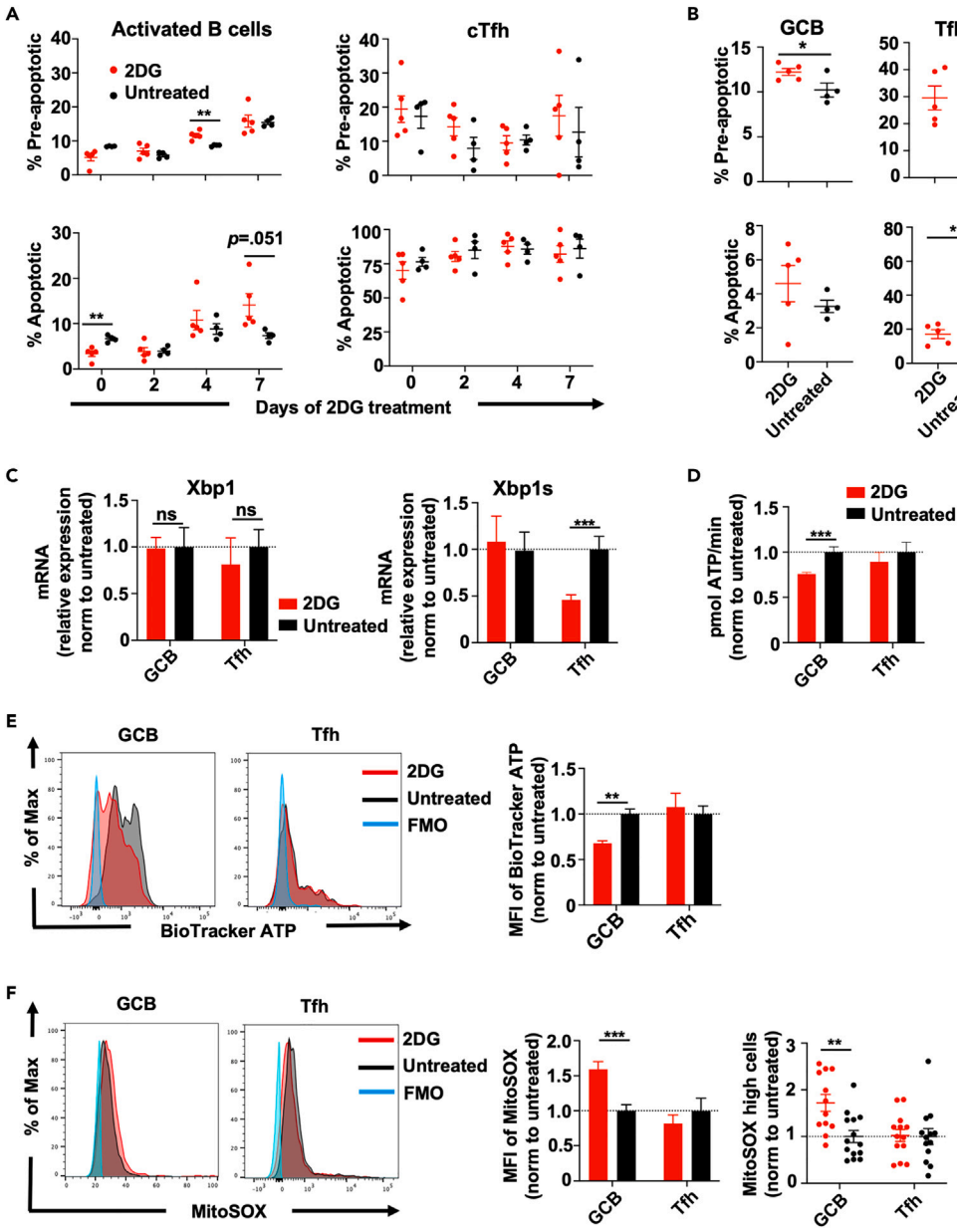

Figure 4. Glycolytic inhibition selectively triggers apoptotic death in activated B and GCB cells

(A and B) Frequencies of apoptotic and pre-apoptotic cells in (A) blood and (B) spleens of *Yaa* DKO mice treated with 2DG for 1 week (n = 4–5 mice per group).

(C and D) Relative *Xbp1* and *Xbp1s* expression in GCB and Tfh cells from *Yaa* DKO mice treated with 2DG for 1 week, normalized to untreated controls. (n = 4–6 mice per group) (D) ATP production rate of GCB and Tfh cells from *Yaa* DKO mice after 2DG treatment, as assessed through Seahorse.

(E) ATP concentration in GCB and Tfh cells from *Yaa* DKO mice treated with 2DG.

(F) MFI and relative frequency of mitochondrial ROS (MitoSOX) in splenic GCB and Tfh cells of *Yaa* DKO mice treated with 2DG for 1 week normalized to untreated controls (n = 14). Data are from at least three independent samples. Each dot represents one mouse. Error bars represent mean ± SEM; ns $p \geq 0.05$, *$p < 0.05$, **$p < 0.01$, ***$p < 0.001$ using one-way ANOVA with Bonferroni's multiple comparison tests (A) or unpaired two-tailed Student's *t*-tests (B–F). See also Figure S5 and Table S1.

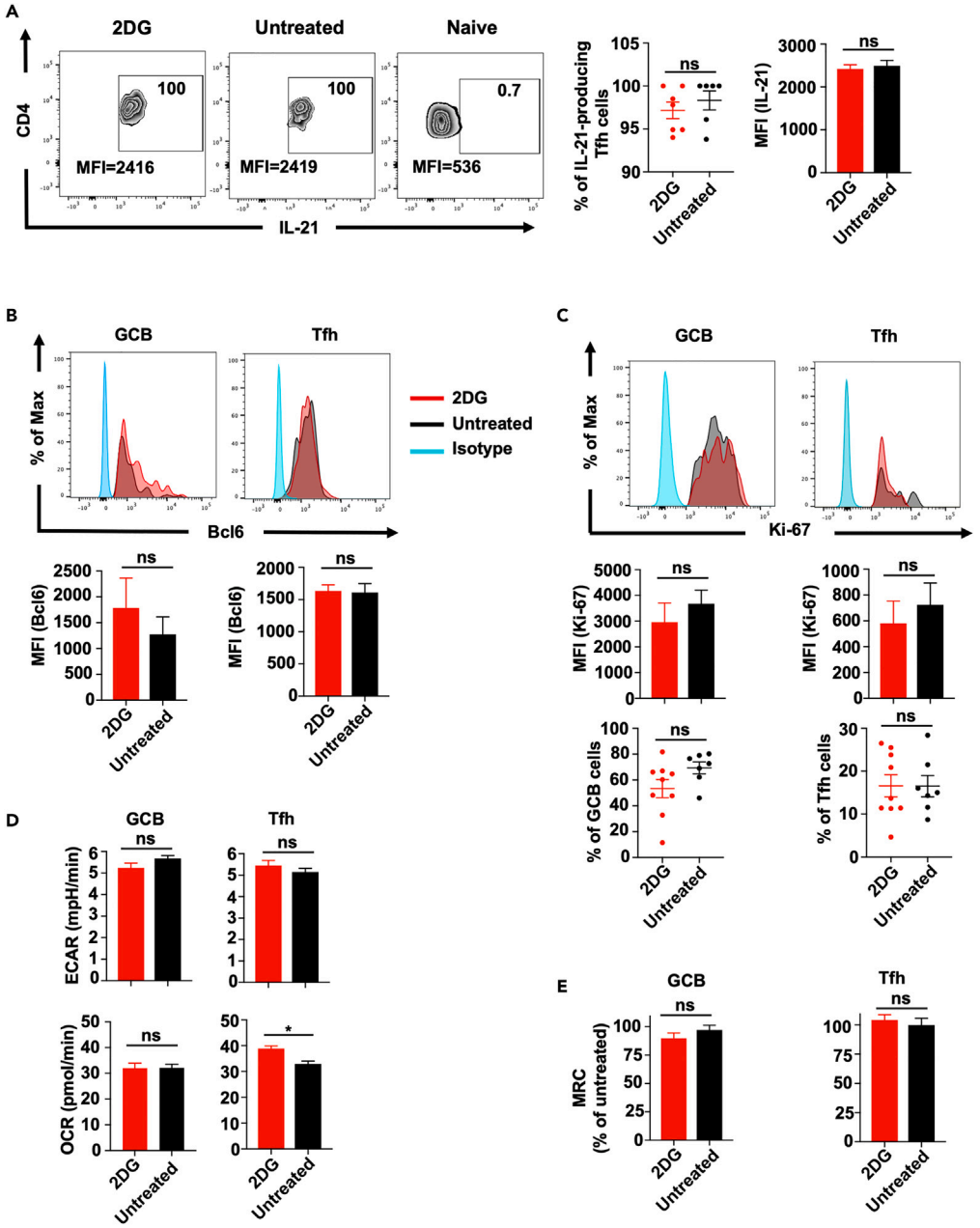

Figure 5. Functionality of Tfh and GCB cells are unaffected by short-term glycolytic inhibition

(A) Flow cytometry of frequencies and expression of IL-21 in splenic Tfh cells from symptomatic *Yaa* DKO mice treated with 1-week 2DG and untreated controls. (n = 6–7 mice per group).

(B) MFI of Bcl6 expression on splenic GCB and Tfh cells from *Yaa* DKO mice treated with 2DG for 1 week or untreated (n = 8–12 mice per group).

(C) Ki-67 expression and frequency of Ki-67^{+} cells in splenic GCB and Tfh cells of *Yaa* DKO mice treated with 2DG for 1 week or untreated (n = 7–9 mice per group).

(D) Basal ECAR, OCR, and (E) maximum respiratory capacity (MRC) in GCB and Tfh cells from 1-week 2DG-treated and untreated *Yaa* DKO mice in response to 2DG injection. 2DG-effect on MRC was normalized to untreated cells and assessed as the contribution of glucose metabolism to OXPHOS (MRC % of untreated) following FCCP exposure. Data are from at least three independent experiments. Each dot represents one mouse. Error bars represent mean ± SEM; ns $p \geq 0.05$, *$p < 0.05$, using unpaired two-tailed Student's *t*-tests. See also Figure S6.

metabolic profiles and the reliance of glucose oxidation in GCB cells were altered after short-term 2DG treatment of mice. The basal ECAR and OCR of GCB cells from mice treated with 2DG were similar to those from untreated mice (Figure 5D). In contrast, basal OCR of Tfh cells was significantly elevated in mice treated with 2DG compared with untreated mice (Figure 5D). These findings suggest that the remaining GCB cells after short-term 2DG treatment were not metabolically compromised and that Tfh cells can better alter their metabolism to survive glycolytic inhibition. Moreover, the reliance on glucose oxidation of the remaining GCB cells from 2DG-treated mice became negligible, as determined by MRC (Figure 5E), indicating that the GCB cells with high reliance on glycolysis were selectively depleted by the 2DG treatment. Overall, these data indicate that short-term glycolytic inhibition selectively targets hyperactive GCB cells with high glycolytic dependency while preserving Tfh and GCB cell functionality, including their metabolic profiles.

BCMA-expressing B cells exhibit elevated glucose dependency and can be targeted to treat lupus

BCMA is a transmembrane glycoprotein expressed on activated B and plasma cells[42] and is associated with disease activity in human lupus.[5,6] Numbers of total peripheral B and activated B cells expressing BCMA (Figure S7A) were significantly elevated in pre-symptomatic and symptomatic *Yaa* DKO mice compared to immunized non-lupus mice or healthy mice, and increased with disease severity (Figures 6A and 6B). Following short-term 2DG treatment, numbers of both circulating BCMA$^+$ activated B cells and splenic BCMA$^+$ GCB cells from symptomatic *Yaa* DKO mice decreased significantly (Figures 6C, 6D, and S7A). We found that BCMA$^+$ GCB cells showed significantly higher surface expression of Glut1 (Figure 6E), and significantly greater 2-NBDG uptake (Figure 6F), as well as higher basal ECAR and OCR rates, compared to BCMA$^-$ GCB cells (Figures 6G and 6H). Interestingly, we also found that BCMA$^+$ GCB cells from lupus mice had a higher bioenergetic demand and glycolytic usage compared to those from immunized mice, as evidenced by lower levels of Glut1, 2-NBDG uptake, and ECAR (Figures 6E–6G). While both BCMA$^+$ and BCMA$^-$ GCB cells from *Yaa* DKO mice exhibited reduced MRC with 2DG treatment, the reduction was significantly greater in BCMA$^+$ GCB cells. Conversely, GCB cells from immunized mice did not exhibit a significant reliance on glucose oxidation, regardless of BCMA expression (Figures 6I and 6J). Together, these data suggest that short-term inhibition of glycolysis with 2DG preferentially targets lupus BCMA$^+$ GCB cells, which are highly bioenergetic and rely more heavily on glucose oxidation.

To further explore the role of activated BCMA$^+$ B cells in disease in greater detail, we used chimeric antigen receptor (CAR)-T cells expressing TNFSF13 (APRIL), which is a very high-affinity ligand for BCMA.[42] By injecting a small number of the APRIL-based CAR-T cells into symptomatic *Yaa* DKO mice with severe clinical disease, we achieved a significant decrease in numbers of circulating activated B cells after 1 week compared with mice treated with empty vector-transduced T cells (Figure 6K). Teff, cTfh, and plasmablasts/plasma cell numbers were not decreased, suggesting the specificity of the CAR-T cells (Figure S7B). Mice treated with APRIL-based CAR-T cells exhibited a significantly prolonged mean lifespan (20.4 weeks) compared to control mice (15.6 weeks) (Figure 6L). Together, these data highlight the significant role of highly glycolytic BCMA$^+$ activated B and GCB cells in lupus pathogenesis and support the potential of targeting these cells with CAR-T cells expressing APRIL as a promising therapeutic strategy.

Transcriptomic analysis shows strong correlation between activated B cells and glycolysis in human SLE

To evaluate whether there is elevated glycolysis in the B-cell over T-cell compartment in human SLE, we analyzed publicly available transcriptomic data (GEO accession: GSE164457) of sorted peripheral CD19$^+$ B and CD4$^+$ T cells from lupus patients.[43] Linear regression analyses revealed that the gene signature of activated B cells had a strong, positive correlation with glycolysis, and weak positive correlations with pentose phosphate pathway, tricarboxylic acid cycle, and OXPHOS, and a weak negative correlation with glutamine metabolism, but no correlation with FAO (Figure 7). Conversely, the activated/effector T-cell gene signature was weakly correlated with both the pentose phosphate pathway and glutamine metabolism, with negative and positive correlations, respectively, but was not correlated with glycolysis, tricarboxylic acid cycle, OXPHOS, or FAO. Notably, there was no significant correlation between the abundance of total B cell signatures and any metabolic pathway. However, total T cells showed a weak negative correlation with both the TCA cycle and OXPHOS. Tfh cells exhibited a weak positive correlation with glycolysis and a weak negative correlation with OXPHOS (Figure 7). When comparing human results to mice, it was noted that peripheral activated B cells from lupus patients and splenic activated B cells of

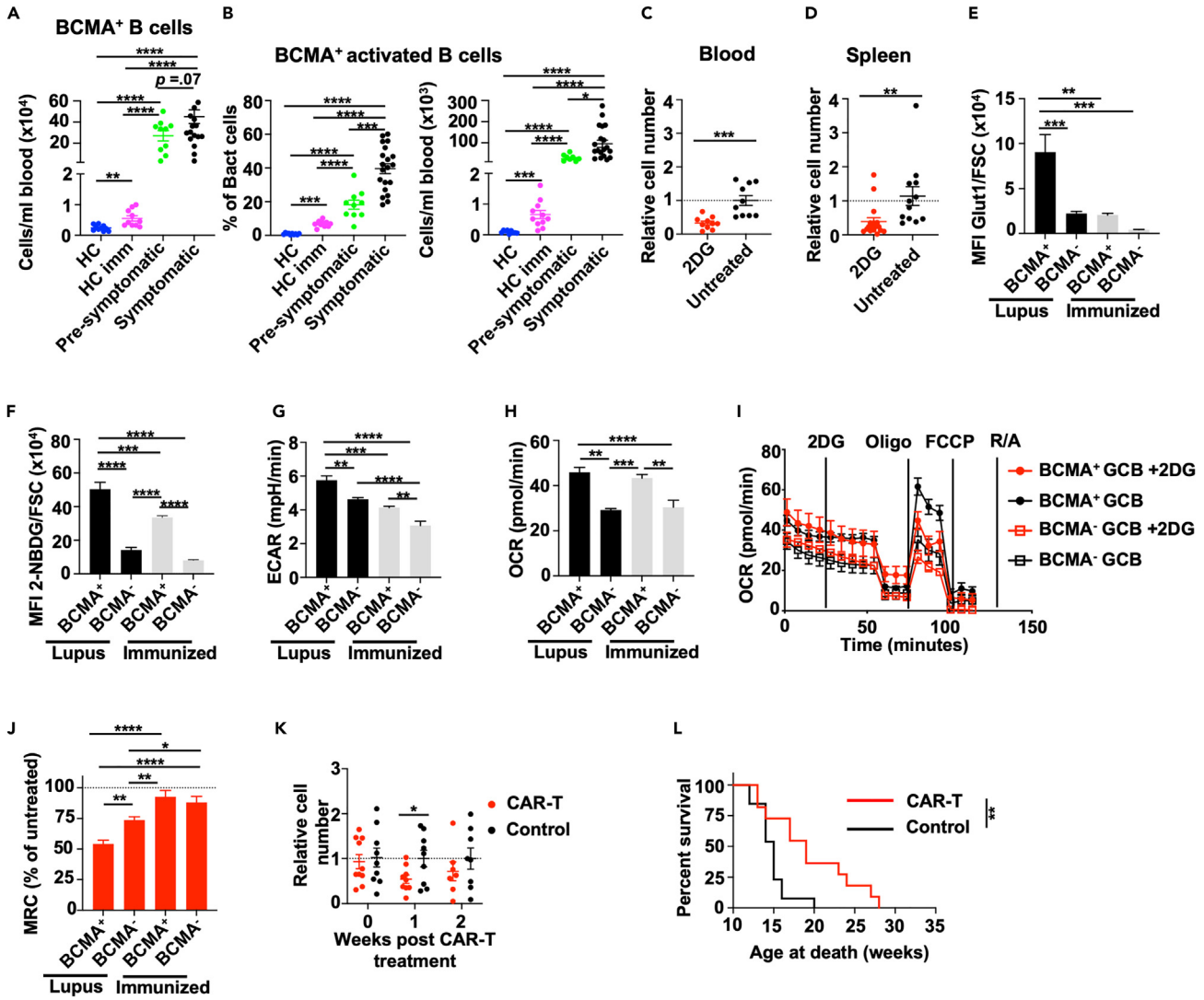

Figure 6. CAR-T cells targeting BCMA reduces activated B cells and increases lifespan of *Yaa* DKO mice

(A-L) All experiments were performed with symptomatic *Yaa* DKO mice, unless otherwise indicated.

(A and B) Frequencies of BCMA expression on peripheral (A) total B cells and (B) activated B cells from pre-symptomatic and symptomatic *Yaa* DKO mice, and healthy immunized and healthy non-immunized B6 mice (n = 10–20 mice per group).

(C and D) Numbers of (C) BCMA$^+$ activated B cells in blood and (D) BCMA$^+$ GCB cells in spleens from mice treated with 2DG for 1 week or untreated, normalized to untreated controls (n = 10–12 mice per group).

(E) Glut1 expression and (F) 2-NBDG uptake in splenic BCMA$^+$ and BCMA$^-$ GCB cells, from *Yaa* DKO and immunized B6 mice normalized to cell size (FSC) (n = 9–10 mice per group).

(G and H) Basal (G) ECAR and (H) OCR of splenic BCMA$^+$ vs. BCMA$^-$ GCB cells from *Yaa* DKO and immunized B6 mice.

(I) OCR and maximum respiratory capacity (MRC) of BCMA$^+$ and BCMA$^-$ GCB cells with or without 2DG before treatment with oligomycin (oligo), FCCP, and rotenone/antimycin (R/A) from *Yaa* DKO mice.

(J) 2DG-effect on MRC was normalized to untreated cells and assessed as the contribution of glucose metabolism to OXPHOS (MRC % of untreated) in BCMA$^+$ and BCMA$^-$ GCB cells from *Yaa* DKO and immunized B6 mice following FCCP exposure.

(K) Relative numbers of peripheral activated B cells normalized to untreated controls and (L) survival of mice treated with APRIL-based CAR-T or empty vector transduced T cells. Each dot represents one mouse (n = 15 mice per group). Data are presented from at least two independent experiments. Error bars represent mean ± SEM; *p < 0.05, **p < 0.01, ***p < 0.001, ****p < 0.0001 using one-way ANOVA with Bonferroni's multiple comparison tests (A–B, E–H, and J–K), Mantel-Cox test (L), or per unpaired two-tailed Student's *t*-tests (C–D). See also Figure S7.

lupus-prone mice (Figures 7 and S1G) were both strongly positively correlated with glycolysis. These findings suggest that elevated glycolysis plays a critical role in activated B cells in human SLE and that short-term glycolytic blockade may be efficacious in preferentially targeting pathogenic activated B cells.

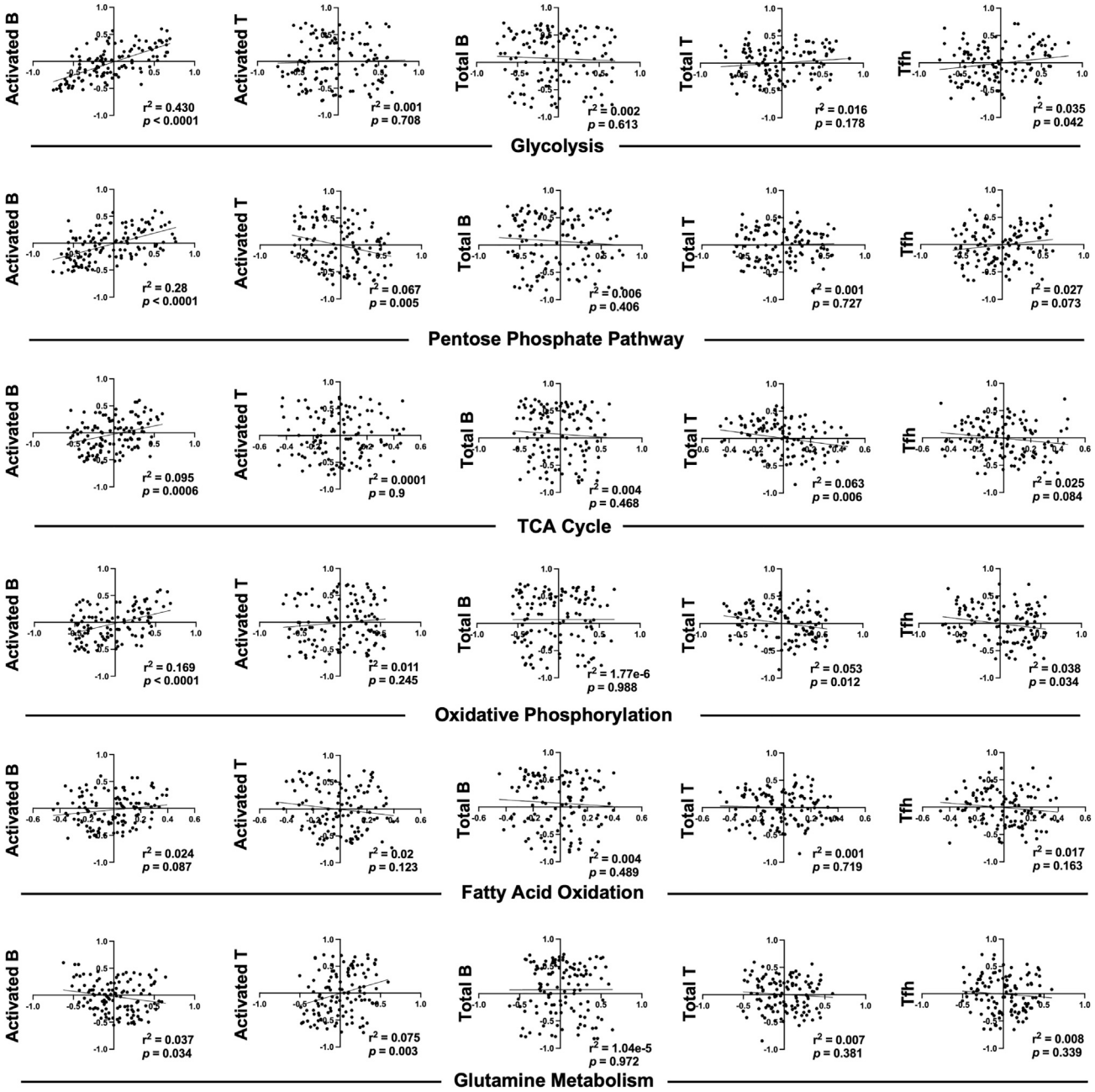

Figure 7. Activated B cells, but not activated T cells from lupus patients are strongly correlated with glycolysis-related genes

Gene-expression data from $CD19^+$ B cells or $CD4^+$ T cells isolated from lupus patients (n = 120 individuals) was used for linear regression between GSVA scores for activated B, activated/effector T, total B, total T, and Tfh cells and metabolic pathway gene signatures. The goodness of fit for each comparison is displayed as the r^2 value and the slope of the regression line is displayed as the p value. Correlations with $p < 0.05$ were considered significant. TCA, tricarboxylic acid. See also Tables S4 and S5.

DISCUSSION

Alterations in glucose metabolism within activated immune/inflammatory cells are increasingly appreciated to underlie lupus and related autoimmune disorders,[44–46] but how such metabolic modifications are differentially manifested in the various cell types that contribute to autoimmune pathogenesis remains obscure. Here, we determined that gene expression signatures for activated B cells are significantly reduced in lupus-prone mice treated with 2DG, whereas signatures for activated/effector T cells are

much less impacted. Moreover, glycolysis pathway-related genes correlate highly with the murine-activated B cell signature, but this is weaker with the activated/effector T cell signature. Interestingly, the glycolysis gene signature also shows a high correlation with peripheral activated B cells in SLE patients compared to those of other metabolic pathways. We further reveal that both activated B cells and GCB cells are highly dependent on glycolysis for survival, but that Tfh cells are more metabolically flexible in meeting their energetic requirements. This glycolytic dependency translates into an exploitable weakness whereby activated B and GCB cells are preferentially targetable via short-term inhibition of glucose oxidation via 2DG. This depletion is correlated with significantly increased lifespan in lupus-prone mice, even those with advanced disease. Furthermore, we demonstrate that highly activated BCMA-expressing GCB cells exhibit heightened glucose metabolism and are exquisitely vulnerable to even short-term inhibition of glucose oxidation. Targeting activated B cells with BCMA-specific CAR-T cells extends the lifespan in symptomatic lupus-prone mice to a similar extent as those treated with short-term 2DG. These findings suggest that glycolytic requirements between activated B and GCB cells, and Tfh cells differ, and that pathogenic activated B cells, including GCB cells, are selective targets of short-term anti-glycolytic therapy, and may provide a new metabolic niche for the treatment of lupus and potentially other autoimmune disorders.

Sustained T cell-B cell interaction has been associated with numerous autoimmune conditions,[2,9] with activated T cells producing pro-inflammatory cytokines that support B-cell activation, expansion, and differentiation into antibody-secreting plasmablasts/plasma cells.[1] Long-term treatment of pre-symptomatic *Yaa* DKO lupus-prone mice with 2DG results in attenuated cellular disease phenotypes in T cells, including Tfh cells, and markedly reduces activated B cells, GCB cells, and plasmablasts/plasma cells. Moreover, 2DG confers complete survival for the duration of the treatment in this acute model of lupus. However, long-term glycolytic inhibition via 2DG has a broad suppressive effect on a number of cell types, increasing the risk of adverse effects and potentially limiting clinical translatability. In addition, the extensive effects resulting from persistent 2DG treatment *in vivo* make it difficult to identify the key pathogenic cell type that is primarily responsible for reduced lupus manifestations induced by glycolytic inhibition. To elucidate this, we show that activated B cells display heightened glycolytic activity (ECAR) over Tfh cells. Specifically, the GCB cell subset of activated B cells exhibits higher Glut1 expression, and a correspondingly increased glucose uptake compared to Tfh cells. Elevated Ki-67 expression in GCB over Tfh cells indicates that these GCB cells are highly proliferative, which further implicates higher glycolytic rates,[14–16] directly supporting previous inferences.[44,46,47] A previous study has assessed the efficacy of long-term 2DG treatment on various autoimmune cell types in B6.NZM-Sle1NZM2410/Aeg Sle2NZM2410/Aeg Sle3NZM2410/Aeg/LmoJ triple congenic (TC) lupus-prone mice at 7 months old and concluded that 2DG alone is insufficient to reverse disease state.18 However, this study did not examine efficacy through survival, but instead focused on CD4 T cells, which we also show to be resistant to 2DG. Another study showed that 2DG reduced Tfh and GCB cell numbers when applied prophylactically over 8 weeks and suggested that the therapeutic efficacy was related to a reduction of Tfh cells.17 Our data indicate that reductions in GCB cells occur before that of Tfh cells, and therapeutic efficacy resulting from GCB cell reductions occurs within 1 week of therapeutic application, even in mice with advanced lupus disease.

Current standard treatment for lupus involves non-specific immunosuppression, which can lead to increased risk of infection and cancer.[45,48] To address this, recent efforts have focused on targeted therapies for lupus to improve efficacy with fewer adverse effects. B cells have been targeted both by belimumab neutralization of B cell survival factor TNFSF13B, and by anti-CD19 CAR-T cells, both of which have provided clinical benefits in human lupus.[8,49,50] However, even these more targeted therapies still leave patients immunocompromised. In this study, we investigate the effects of short-term inhibition of glucose oxidation with 2DG on acute (*Yaa* DKO) and chronic (NZBWF1) lupus mice with severe clinical disease and show that this treatment selectively affects pathogenic activated B and GCB cells, leading to significantly extended lifespans of both models. Interestingly, our findings deviate from a previous study using a B6 kika mouse model carrying a human TLR7 mutant variant, which showed that the lack of GC development did not affect lupus progression, and instead identified extrafollicular B cells as a critical driver in that model.[51] However, we found that our therapeutic efficacy with short-term inhibition of glucose oxidation using 2DG did not involve reducing extrafollicular B cells, highlighting the heterogeneity of lupus disease. Similarly, in *Yaa* DKO mice, decreased GCB cells with 2DG treatment coincide with a decrease in GC size but not in GC numbers. Since Tfh cells control GC initiation and survival,[10–12] and we show that these cells are not significantly affected by short-term 2DG treatment, the lack of change in GC numbers is not

unexpected. However, in NZBWF1 mice, we observed a significant reduction in GCB cell numbers with 2DG treatment, but no corresponding decrease in GC size. This lack of correlation between GCB-cell numbers and GC size suggests that other environmental cues may be affecting GC size, such as the numbers of follicular regulatory T cells,[52] the expression of sphingosine 1-phosphate receptor type 2,[53] or the levels of cytokines or growth factors that sustain GC size, such as IL-4, IL-6, and IL-21.[38,54,55] Further studies are needed to elucidate the potential mechanisms that contribute to the differences in GC morphology between these lupus mouse models.

Our study also provides a potential mechanistic explanation by which 2DG reverses abnormal immunophenotypes *in vivo*. We found that glycolytic inhibition reduces ATP production in GCB cells from lupus mice, leading to an increase in mitochondrial ROS-mediated metabolic oxidative stress and subsequent apoptosis. This suggests that the increased glycolytic reliance of GCB cells may be an adaptation to compensate for excessive ROS production.[56] While increased ROS is typically associated with an increase in OCR, we observe the opposite effect, which has been previously reported[57,58] and attributed to impaired mitochondrial function caused by enzyme inactivation or decreased antioxidants responsible for detoxifying ROS.[58,59] This supports the idea that 2DG impairs mitochondrial function in GCB cells that lack the metabolic flexibility to oxidize other fuels to compensate for glycolytic blockade. To definitively demonstrate that increased oxidative stress and ROS production in GCB cells following 2DG treatment is the mechanism behind 2DG-induced reduction of activated B and GCB cells, further intensive studies are needed. Elucidating this is complicated by the constitutive expression of CD95 on GCB cells[28–30] as CD95 plays a role in controlling apoptosis,[60] but can also induce cell survival,[61,62] proliferation,[63,64] differentiation,[65] homing,[66] and co-stimulation,[60,61] and is modulated by various factors such as phosphorylation, ubiquitination, and protein binding.[67] Therefore, further intensive studies are needed to elucidate the exact mechanism behind 2DG-induced reductions in these cells. Conversely, our findings suggest that Tfh cells exhibit a greater degree of metabolic flexibility to compensate for fuel oxidation during glycolytic restriction, which allow them to maintain ATP production and survive with unimpeded functionality. Furthermore, the lack of glycolytic dependency in GCB cells from mice after short-term 2DG treatment points to the targeted reduction of GCB cells with higher glycolytic reliance, sparing those with lesser demand. The evidence of prolonged lifespan of lupus-prone mice with this short 2DG treatment course, paired with the dampening of this effect after the transfer of activated B cells, including GCB cells, indicates that these glycolysis-dependent cells are pathogenic and that 2DG can target these pathogenic populations, thereby avoiding a pan reduction of B and T cells that would render the immune system compromised. In addition, the lack of a strong effect on the activated/effector T cell and Tfh cell gene signatures in long-term 2DG-treated mice raises the question of the primary mechanism of this glycolytic restriction, especially in view of the interdependency of Tfh and GCB cells.[1,9] This presents the possibility that the observed reductions of Tfh cells after prophylactic, long-term 2DG treatment may not stem from a direct effect of 2DG on Tfh cells, but rather from a lack of costimulatory signaling from GCB cells after their depletion via 2DG. Overall, our study highlights the potential of 2DG as a targeted therapeutic approach to reduce pathogenic B cell populations in lupus without compromising overall immune function.

Our findings emphasize the importance of activated B and GCB cells in driving disease pathogenesis and highlight them as the prime target of anti-glycolytic therapy. We have found that the subset of BCMA-expressing GCB cells in lupus-prone mice displays an extremely high reliance on glycolysis and sensitivity to 2DG. BCMA is overexpressed on both human and murine circulating B cells during lupus progression,[6,68] and its ligation is involved in increased expression of the anti-apoptotic gene, *Mcl-1*, in B cells committed to differentiation into long-lived plasma cells.[69,70] This sustained survival and resistance to apoptosis can exacerbate autoimmunity. Here, we show that elevated BCMA expression on GCB cells from *Yaa* DKO mice, which is reduced after short-term 2DG treatment, is associated with elevated Glut1 expression, glucose uptake, and elevated glycolytic requirements. $BCMA^+$ GCB cells generated in response to foreign antigen immunization also show increased Glut1 expression and glucose uptake over $BCMA^-$ GCB cells, but $BCMA^+$ GCB from lupus mice exhibit significantly greater glycolytic demand, underscoring their hyperactivated nature in autoimmunity. Our observations suggest that dysregulated glucose metabolism may contribute to the pathogenesis of lupus in $BCMA^+$ GCB cells, highlighting a potential link between metabolic dysregulation and autoimmune diseases. Glycolytic inhibition has been reported to decrease Mcl-1 synthesis via promoting the AMPK-mTOR pathway.[71] Understanding the regulation of Mcl-1 levels by glucose metabolism may be a critical aspect of appreciating how glycolytic blockade can differentially affect activated B and GCB cell survival. Given their augmented glycolysis usage and association with

lupus, circulating BCMA-expressing activated B cells might serve as a sensitive indicator for the efficacy of glycolytic blockade therapy. Our APRIL-based CAR-T cell treatment yielded enhanced survival in treated mice, similar to short-term inhibition of glucose oxidation with 2DG, further validating the importance of BCMA-expressing activated B cells in lupus pathology. Paired with increased frequencies of $BCMA^+$ B cells in lupus patients,[5,6] hyperactivated BCMA-expressing activated B and GCB cells may be a central B cell population involved in lupus pathogenesis.

Our findings that autoimmune GCB cells rely heavily on glucose oxidation differ from those described in an immunization paradigm, in which GCB cells isolated from 4-Hydroxy-3-nitrophenylacetyl hapten-conjugated to chicken gamma globulin (NP-CGG) immunized mice exhibit very low rates of glycolysis and instead rely mainly on FAO to meet their energetic demands.[28] Moreover, previous studies have demonstrated that autoimmune mice treated with long-term 2DG and immunized with NP-conjugated to keyhole limpet hemocyanin (NP-KLH) maintained a robust GC response against the exogenous antigen.[17] Our data are consistent with these findings as GCB cells isolated from non-autoimmune immunized mice did not exhibit a reliance on glycolysis. This suggests that the response of GCB cells to foreign antigens is refractory to conditions that induce apoptosis in autoreactive GCB cells, indicating a major disparity in energy requirements between the two activated B-cell types. One possible explanation for this discrepancy is that chronic autoantigen stimulation in autoimmunity could cause immune cells to become increasingly activated as disease progresses, versus the more acute stimulation resulting from exposure to a foreign antigen. Further studies are needed to understand this metabolic divergence between autoimmune- and immunization-induced GCB cells.

Overall, our results illustrate that activated B and GCB cells have a greater glycolytic dependency and activated B cells and GCB cells manifest apoptotic sensitivity to glycolysis inhibition compared with Tfh cells. We further demonstrate that a short-term inhibition of glucose oxidation with 2DG specifically targets BCMA-expressing activated B and GCB cells with high glycolytic dependency, and that the reduction of this subset confers significant lifespan extension, all while preserving the number and function of other examined immune cells. Further studies will determine how the restrictive glycolytic requirement of these activated B and GCB cells contributes to GC formation and maintenance in autoimmunity, and whether this metabolic switch links to crucial transcription factor programs. Future treatments designed to target these pathogenic activated B and GCB cells, including short-term glycolytic inhibition and CAR-T cells, may improve the outcomes of patients with lupus and other autoimmune disorders.

Limitations of the study

Our analysis of publicly available gene expression data from sorted T and B cells of lupus patients reveals a stronger correlation between activated B cells and glycolysis compared to Tfh cells. This correlation is also stronger than with any other metabolic pathway, which is consistent with findings from our mouse studies. Further investigation using sorted autoreactive cells from lupus patients alongside vaccine-induced activate B cells from healthy individuals would provide valuable insights into the metabolic differences between autoimmune and foreign antigen-stimulated cells. Whereas there is strong evidence for the reduction of activated B cells, including GCB cells, playing a major role in 2DG treatment efficacy, other non-T or B cell types might also be involved. Mice treated with 2DG and then injected with activated B and GCB cells lived ~3.5 weeks less than untreated mice. Moreover, CAR-T therapy reducing $BCMA^+$ B cells also resulted in an increased lifespan that was ~3.5 weeks shorter than the increase induced by 1-week 2DG treatment. This could indicate that an increased number of CAR-T cells are needed to further increase survival, or that other, non-T/B cell populations could be functionally affected by glycolytic inhibition and are partially contributing to the observed therapeutic efficacy. For example, macrophages from mice modeling septic shock showed impaired tumor necrosis factor-alpha production after intraperitoneal injection of 2DG, demonstrating a reduction in macrophage proinflammatory signaling.[72] Moreover, plasmablasts/plasma cells, which are known to be highly glycolytic[28,73] and express BCMA,[6,70] experience a significant reduction following long-term prophylactic 2DG treatment. Although the numbers of these cells are not significantly altered in either short-term 2DG or APRIL CAR-T treatment, there were numerical trends toward their reduction after both treatments. These trends may partially contribute in part to the therapeutic efficacy observed with 2DG and CAR-T therapies and future studies are needed to explore these possibilities. Moreover, additional studies are required to elucidate the precise mechanism of how the depletion of $GL7^+$ activated B and GCB cells specifically alters lupus pathology to increase lifespan.

STAR★METHODS

Detailed methods are provided in the online version of this paper and include the following:

- KEY RESOURCES TABLE
- RESOURCE AVAILABILITY
  - Lead contact
  - Materials availability
  - Data and code availability
- EXPERIMENTAL MODEL AND SUBJECT DETAILS
  - Mice and treatments
- METHOD DETAILS
  - Flow cytometry and intracellular staining
  - Cell survival assays
  - Metabolic assays
  - Immunohistochemistry
  - Gene expression analysis by RNA-sequencing and quantitative real-time PCR
  - Gene set variation analysis (GSVA)
  - GSVA gene set generation and co-expression analysis
  - Retrovirus vector designs and generation of APRIL-based CAR-T cells
  - Adoptive transfer
- QUANTIFICATION AND STATISTICAL ANALYSIS
  - Statistical analysis

SUPPLEMENTAL INFORMATION

Supplemental information can be found online at https://doi.org/10.1016/j.isci.2023.107487.

ACKNOWLEDGMENTS

We thank Will Schott, Danielle Littlefield, and Krystal-Leigh Brown for procedural expertise with flow cytometry experiments, Philipp Henrich for technical assistance with fluorescent imaging, Karolina Palucka, Guangwen Ren, and David Serreze for reagents and advice, and Edison Liu for critical review, and Stephen Sampson for critical editing of the manuscript. This work was funded by The Jackson Laboratory Director's Innovation Fund (19000-18-19 and 19000-21-07) and the US Department of Defense (HT9425-23-1-0308) to CC, and supported by the RILITE Foundation, and the John and Marcia Goldman Foundation to PEL.

AUTHOR CONTRIBUTIONS

J.J.W., J.W., L.B., A.C.G., P.E.L., D.C.R., and C.C. designed the research. J.J.W., J.W., J.D.S., E.B., C.L.M., and C.H.C. performed experiments and analyzed data. L.B., A.C.G., and C.C. gave conceptual advice. A.R.D. and G.A.S. performed computational analysis. All authors contributed to writing the manuscript.

DECLARATION OF INTERESTS

Authors declare that they have no competing interests.

Received: November 16, 2022
Revised: March 27, 2023
Accepted: July 24, 2023
Published: July 27, 2023

REFERENCES

1. Domeier, P.P., Schell, S.L., and Rahman, Z.S.M. (2017). Spontaneous germinal centers and autoimmunity. Autoimmunity *50*, 4–18. https://doi.org/10.1080/08916934.2017.1280671.

2. Nutt, S.L., and Tarlinton, D.M. (2011). Germinal center B and follicular helper T cells: siblings, cousins or just good friends? Nat. Immunol. *12*, 472–477. https://doi.org/10.1038/ni.2019.

3. Tsokos, G.C. (2020). Autoimmunity and organ damage in systemic lupus erythematosus. Nat. Immunol. *21*, 605–614. https://doi.org/10.1038/s41590-020-0677-6.

4. Crow, M.K. (2014). Type I interferon in the pathogenesis of lupus. J. Immunol. *192*, 5459–5468. https://doi.org/10.4049/jimmunol.1002795.

5. Salazar-Camarena, D.C., Palafox-Sánchez, C.A., Cruz, A., Marín-Rosales, M., and Muñoz-Valle, J.F. (2020). Analysis of the receptor BCMA as a biomarker in systemic lupus

erythematosus patients. Sci. Rep. *10*, 6236. https://doi.org/10.1038/s41598-020-63390-0.

6. Kim, J., Gross, J.A., Dillon, S.R., Min, J.K., and Elkon, K.B. (2011). Increased BCMA expression in lupus marks activated B cells, and BCMA receptor engagement enhances the response to TLR9 stimulation. Autoimmunity *44*, 69–81. https://doi.org/10.3109/08916934.2010.509122.

7. Vital, E.M., Merrill, J.T., Morand, E.F., Furie, R.A., Bruce, I.N., Tanaka, Y., Manzi, S., Kalunian, K.C., Kalyani, R.N., Streicher, K., et al. (2022). Anifrolumab efficacy and safety by type I interferon gene signature and clinical subgroups in patients with SLE: post hoc analysis of pooled data from two phase III trials. Ann. Rheum. Dis. *81*, 951–961. https://doi.org/10.1136/annrheumdis-2021-221425.

8. Navarra, S.V., Guzmán, R.M., Gallacher, A.E., Hall, S., Levy, R.A., Jimenez, R.E., Li, E.K.M., Thomas, M., Kim, H.Y., León, M.G., et al. (2011). Efficacy and safety of belimumab in patients with active systemic lupus erythematosus: a randomised, placebo-controlled, phase 3 trial. Lancet *377*, 721–731. https://doi.org/10.1016/S0140-6736(10)61354-2.

9. Ise, W., Fujii, K., Shiroguchi, K., Ito, A., Kometani, K., Takeda, K., Kawakami, E., Yamashita, K., Suzuki, K., Okada, T., and Kurosaki, T. (2018). T Follicular Helper Cell-Germinal Center B Cell Interaction Strength Regulates Entry into Plasma Cell or Recycling Germinal Center Cell Fate. Immunity *48*, 702–715.e4. https://doi.org/10.1016/j.immuni.2018.03.027.

10. Zhang, X., Lindwall, E., Gauthier, C., Lyman, J., Spencer, N., Alarakhia, A., Fraser, A., Ing, S., Chen, M., Webb-Detiege, T., et al. (2015). Circulating CXCR5+CD4+helper T cells in systemic lupus erythematosus patients share phenotypic properties with germinal center follicular helper T cells and promote antibody production. Lupus *24*, 909–917. https://doi.org/10.1177/0961203314567750.

11. Terrier, B., Costedoat-Chalumeau, N., Garrido, M., Geri, G., Rosenzwajg, M., Musset, L., Klatzmann, D., Saadoun, D., and Cacoub, P. (2012). Interleukin 21 correlates with T cell and B cell subset alterations in systemic lupus erythematosus. J. Rheumatol. *39*, 1819–1828. https://doi.org/10.3899/jrheum.120468.

12. Dolff, S., Abdulahad, W.H., Westra, J., Doornbos-van der Meer, B., Limburg, P.C., Kallenberg, C.G.M., and Bijl, M. (2011). Increase in IL-21 producing T-cells in patients with systemic lupus erythematosus. Arthritis Res. Ther. *13*, R157. https://doi.org/10.1186/ar3474.

13. Gigoux, M., Shang, J., Pak, Y., Xu, M., Choe, J., Mak, T.W., and Suh, W.K. (2009). Inducible costimulator promotes helper T-cell differentiation through phosphoinositide 3-kinase. Proc. Natl. Acad. Sci. USA *106*, 20371–20376. https://doi.org/10.1073/pnas.0911573106.

14. Pearce, E.L., and Pearce, E.J. (2013). Metabolic pathways in immune cell activation and quiescence. Immunity *38*, 633–643. https://doi.org/10.1016/j.immuni.2013.04.005.

15. Caro-Maldonado, A., Wang, R., Nichols, A.G., Kuraoka, M., Milasta, S., Sun, L.D., Gavin, A.L., Abel, E.D., Kelsoe, G., Green, D.R., and Rathmell, J.C. (2014). Metabolic reprogramming is required for antibody production that is suppressed in anergic but exaggerated in chronically BAFF-exposed B cells. J. Immunol. *192*, 3626–3636. https://doi.org/10.4049/jimmunol.1302062.

16. Chang, C.H., Curtis, J.D., Maggi, L.B., Jr., Faubert, B., Villarino, A.V., O'Sullivan, D., Huang, S.C.C., van der Windt, G.J.W., Blagih, J., Qiu, J., et al. (2013). Posttranscriptional control of T cell effector function by aerobic glycolysis. Cell *153*, 1239–1251. https://doi.org/10.1016/j.cell.2013.05.016.

17. Choi, S.C., Titov, A.A., Abboud, G., Seay, H.R., Brusko, T.M., Roopenian, D.C., Salek-Ardakani, S., and Morel, L. (2018). Inhibition of glucose metabolism selectively targets autoreactive follicular helper T cells. Nat. Commun. *9*, 4369. https://doi.org/10.1038/s41467-018-06686-0.

18. Yin, Y., Choi, S.C., Xu, Z., Perry, D.J., Seay, H., Croker, B.P., Sobel, E.S., Brusko, T.M., and Morel, L. (2015). Normalization of CD4+ T cell metabolism reverses lupus. Sci. Transl. Med. *7*, 274ra18. https://doi.org/10.1126/scitranslmed.aaa0835.

19. McPhee, C.G., Sproule, T.J., Shin, D.M., Bubier, J.A., Schott, W.H., Steinbuck, M.P., Avenesyan, L., Morse, H.C., 3rd, and Roopenian, D.C. (2011). MHC class I family proteins retard systemic lupus erythematosus autoimmunity and B cell lymphomagenesis. J. Immunol. *187*, 4695–4704. https://doi.org/10.4049/jimmunol.1101776.

20. Barwick, B.G., Scharer, C.D., Martinez, R.J., Price, M.J., Wein, A.N., Haines, R.R., Bally, A.P.R., Kohlmeier, J.E., and Boss, J.M. (2018). B cell activation and plasma cell differentiation are inhibited by de novo DNA methylation. Nat. Commun. *9*, 1900. https://doi.org/10.1038/s41467-018-04234-4.

21. Tang, C.H.A., Lee, A.C., Chang, S., Xu, Q., Shao, A., Lo, Y., Spalek, W.T., Pinilla-Ibarz, J.A., Del Valle, J.R., and Hu, C.C.A. (2021). STING regulates BCR signaling in normal and malignant B cells. Cell. Mol. Immunol. *18*, 1016–1031. https://doi.org/10.1038/s41423-020-00552-0.

22. Catalina, M.D., Bachali, P., Yeo, A.E., Geraci, N.S., Petri, M.A., Grammer, A.C., and Lipsky, P.E. (2020). Patient ancestry significantly contributes to molecular heterogeneity of systemic lupus erythematosus. JCI Insight *5*, e140380. https://doi.org/10.1172/jci.insight.140380.

23. Suárez-Fueyo, A., Bradley, S.J., and Tsokos, G.C. (2016). T cells in Systemic Lupus Erythematosus. Curr. Opin. Immunol. *43*, 32–38. https://doi.org/10.1016/j.coi.2016.09.001.

24. Subramanian, A., Tamayo, P., Mootha, V.K., Mukherjee, S., Ebert, B.L., Gillette, M.A., Paulovich, A., Pomeroy, S.L., Golub, T.R., Lander, E.S., and Mesirov, J.P. (2005). Gene set enrichment analysis: a knowledge-based approach for interpreting genome-wide expression profiles. Proc Natl Acad Sci USA *102*, 15545–15550. https://doi.org/10.1073/pnas.0506580102.

25. Mootha, V.K., Lindgren, C.M., Eriksson, K.F., Subramanian, A., Sihag, S., Lehar, J., Puigserver, P., Carlsson, E., Ridderstråle, M., Laurila, E., et al. (2003). PGC-1alpha-responsive genes involved in oxidative phosphorylation are coordinately downregulated in human diabetes. Nat. Genet. *34*, 267–273. https://doi.org/10.1038/ng1180.

26. Hänzelmann, S., Castelo, R., and Guinney, J. (2013). GSVA: gene set variation analysis for microarray and RNA-seq data. BMC Bioinf. *14*, 7. https://doi.org/10.1186/1471-2105-14-7.

27. Daamen, A.R., Wang, H., Bachali, P., Shen, N., Kingsmore, K.M., Robl, R.D., Grammer, A.C., Fu, S.M., and Lipsky, P.E. (2023). Molecular mechanisms governing the progression of nephritis in lupus prone mice and human lupus patients. Front. Immunol. *14*, 1147526. https://doi.org/10.3389/fimmu.2023.1147526.

28. Weisel, F.J., Mullett, S.J., Elsner, R.A., Menk, A.V., Trivedi, N., Luo, W., Wikenheiser, D., Hawse, W.F., Chikina, M., Smita, S., et al. (2020). Germinal center B cells selectively oxidize fatty acids for energy while conducting minimal glycolysis. Nat. Immunol. *21*, 331–342. https://doi.org/10.1038/s41590-020-0598-4.

29. Andersen, T.K., Huszthy, P.C., Gopalakrishnan, R.P., Jacobsen, J.T., Fauskanger, M., Tveita, A.A., Grødeland, G., and Bogen, B. (2019). Enhanced germinal center reaction by targeting vaccine antigen to major histocompatibility complex class II molecules. NPJ Vaccines *4*, 9. https://doi.org/10.1038/s41541-019-0101-0.

30. Sun, D., Stopka-Farooqui, U., Barry, S., Aksoy, E., Parsonage, G., Vossenkämper, A., Capasso, M., Wan, X., Norris, S., Marshall, J.L., et al. (2019). Aryl Hydrocarbon Receptor Interacting Protein Maintains Germinal Center B Cells through Suppression of BCL6 Degradation. Cell Rep. *27*, 1461–1471.e4. https://doi.org/10.1016/j.celrep.2019.04.014.

31. Bengsch, B., Johnson, A.L., Kurachi, M., Odorizzi, P.M., Pauken, K.E., Attanasio, J., Stelekati, E., McLane, L.M., Paley, M.A., Delgoffe, G.M., and Wherry, E.J. (2016). Bioenergetic Insufficiencies Due to Metabolic Alterations Regulated by the Inhibitory Receptor PD-1 Are an Early Driver of CD8(+) T Cell Exhaustion. Immunity *45*, 358–373. https://doi.org/10.1016/j.immuni.2016.07.008.

32. Qie, S., Yoshida, A., Parnham, S., Oleinik, N., Beeson, G.C., Beeson, C.C., Ogretmen, B., Bass, A.J., Wong, K.K., Rustgi, A.K., and Diehl, J.A. (2019). Targeting glutamine-addiction and overcoming CDK4/6 inhibitor resistance in human esophageal squamous cell carcinoma. Nat. Commun. *10*, 1296. https://doi.org/10.1038/s41467-019-09179-w.

33. Aft, R.L., Zhang, F.W., and Gius, D. (2002). Evaluation of 2-deoxy-D-glucose as a chemotherapeutic agent: mechanism of cell death. Br. J. Cancer *87*, 805–812. https://doi.org/10.1038/sj.bjc.6600547.

34. Song, M., Sandoval, T.A., Chae, C.S., Chopra, S., Tan, C., Rutkowski, M.R., Raundhal, M., Chaurio, R.A., Payne, K.K., Konrad, C., et al. (2018). IRE1alpha-XBP1 controls T cell function in ovarian cancer by regulating mitochondrial activity. Nature *562*, 423–428. https://doi.org/10.1038/s41586-018-0597-x.

35. van Schadewijk, A., van't Wout, E.F.A., Stolk, J., and Hiemstra, P.S. (2012). A quantitative method for detection of spliced X-box binding protein-1 (XBP1) mRNA as a measure of endoplasmic reticulum (ER) stress. Cell Stress Chaperones *17*, 275–279. https://doi.org/10.1007/s12192-011-0306-2.

36. Simons, A.L., Mattson, D.M., Dornfeld, K., and Spitz, D.R. (2009). Glucose deprivation-induced metabolic oxidative stress and cancer therapy. J. Cancer Res. Ther. *5* (*Suppl 1*), S2–S6. https://doi.org/10.4103/0973-1482.55133.

37. Spitz, D.R., Sim, J.E., Ridnour, L.A., Galoforo, S.S., and Lee, Y.J. (2000). Glucose deprivation-induced oxidative stress in human tumor cells. A fundamental defect in metabolism? Ann. N. Y. Acad. Sci. *899*, 349–362. https://doi.org/10.1111/j.1749-6632.2000.tb06199.x.

38. Arkatkar, T., Du, S.W., Jacobs, H.M., Dam, E.M., Hou, B., Buckner, J.H., Rawlings, D.J., and Jackson, S.W. (2017). B cell-derived IL-6 initiates spontaneous germinal center formation during systemic autoimmunity. J. Exp. Med. *214*, 3207–3217. https://doi.org/10.1084/jem.20170580.

39. Jain, S., Park, G., Sproule, T.J., Christianson, G.J., Leeth, C.M., Wang, H., Roopenian, D.C., and Morse, H.C., 3rd (2016). Interleukin 6 Accelerates Mortality by Promoting the Progression of the Systemic Lupus Erythematosus-Like Disease of BXSB.Yaa Mice. PLoS One *11*, e0153059. https://doi.org/10.1371/journal.pone.0153059.

40. Nurieva, R.I., Chung, Y., Martinez, G.J., Yang, X.O., Tanaka, S., Matskevitch, T.D., Wang, Y.H., and Dong, C. (2009). Bcl6 mediates the development of T follicular helper cells. Science *325*, 1001–1005. https://doi.org/10.1126/science.1176676.

41. Dent, A.L., Shaffer, A.L., Yu, X., Allman, D., and Staudt, L.M. (1997). Control of inflammation, cytokine expression, and germinal center formation by BCL-6. Science *276*, 589–592. https://doi.org/10.1126/science.276.5312.589.

42. Schmidts, A., Ormhøj, M., Choi, B.D., Taylor, A.O., Bouffard, A.A., Scarfò, I., Larson, R.C., Frigault, M.J., Gallagher, K., Castano, A.P., et al. (2019). Rational design of a trimeric APRIL-based CAR-binding domain enables efficient targeting of multiple myeloma. Blood Adv. *3*, 3248–3260. https://doi.org/10.1182/bloodadvances.2019000703.

43. Andreoletti, G., Lanata, C.M., Trupin, L., Paranjpe, I., Jain, T.S., Nititham, J., Taylor, K.E., Combes, A.J., Maliskova, L., Ye, C.J., et al. (2021). Transcriptomic analysis of immune cells in a multi-ethnic cohort of systemic lupus erythematosus patients identifies ethnicity- and disease-specific expression signatures. Commun. Biol. *4*, 488. https://doi.org/10.1038/s42003-021-02000-9.

44. Teng, X., Cornaby, C., Li, W., and Morel, L. (2019). Metabolic regulation of pathogenic autoimmunity: therapeutic targeting. Curr. Opin. Immunol. *61*, 10–16. https://doi.org/10.1016/j.coi.2019.07.001.

45. Rhoads, J.P., Major, A.S., and Rathmell, J.C. (2017). Fine tuning of immunometabolism for the treatment of rheumatic diseases. Nat. Rev. Rheumatol. *13*, 313–320. https://doi.org/10.1038/nrrheum.2017.54.

46. Perl, A. (2016). Activation of mTOR (mechanistic target of rapamycin) in rheumatic diseases. Nat. Rev. Rheumatol. *12*, 169–182. https://doi.org/10.1038/nrrheum.2015.172.

47. Galgani, M., Bruzzaniti, S., and Matarese, G. (2020). Immunometabolism and autoimmunity. Curr. Opin. Immunol. *67*, 10–17. https://doi.org/10.1016/j.coi.2020.07.002.

48. Mazumdar, C., Driggers, E.M., and Turka, L.A. (2020). The Untapped Opportunity and Challenge of Immunometabolism: A New Paradigm for Drug Discovery. Cell Metab. *31*, 26–34. https://doi.org/10.1016/j.cmet.2019.11.014.

49. Mackensen, A., Müller, F., Mougiakakos, D., Böltz, S., Wilhelm, A., Aigner, M., Völkl, S., Simon, D., Kleyer, A., Munoz, L., et al. (2022). Anti-CD19 CAR T cell therapy for refractory systemic lupus erythematosus. Nat. Med. *28*, 2124–2132. https://doi.org/10.1038/s41591-022-02017-5.

50. Mougiakakos, D., Krönke, G., Völkl, S., Kretschmann, S., Aigner, M., Kharboutli, S., Böltz, S., Manger, B., Mackensen, A., and Schett, G. (2021). CD19-Targeted CAR T Cells in Refractory Systemic Lupus Erythematosus. N. Engl. J. Med. *385*, 567–569. https://doi.org/10.1056/NEJMc2107725.

51. Brown, G.J., Cañete, P.F., Wang, H., Medhavy, A., Bones, J., Roco, J.A., He, Y., Qin, Y., Cappello, J., Ellyard, J.I., et al. (2022). TLR7 gain-of-function genetic variation causes human lupus. Nature *605*, 349–356. https://doi.org/10.1038/s41586-022-04642-z.

52. Linterman, M.A., Pierson, W., Lee, S.K., Kallies, A., Kawamoto, S., Rayner, T.F., Srivastava, M., Divekar, D.P., Beaton, L., Hogan, J.J., et al. (2011). Foxp3+ follicular regulatory T cells control the germinal center response. Nat. Med. *17*, 975–982. https://doi.org/10.1038/nm.2425.

53. Green, J.A., Suzuki, K., Cho, B., Willison, L.D., Palmer, D., Allen, C.D.C., Schmidt, T.H., Xu, Y., Proia, R.L., Coughlin, S.R., and Cyster, J.G. (2011). The sphingosine 1-phosphate receptor S1P(2) maintains the homeostasis of germinal center B cells and promotes niche confinement. Nat. Immunol. *12*, 672–680. https://doi.org/10.1038/ni.2047.

54. Zotos, D., Quast, I., Li-Wai-Suen, C.S.N., McKenzie, C.I., Robinson, M.J., Kan, A., Smyth, G.K., Hodgkin, P.D., and Tarlinton, D.M. (2021). The concerted change in the distribution of cell cycle phases and zone composition in germinal centers is regulated by IL-21. Nat. Commun. *12*, 7160. https://doi.org/10.1038/s41467-021-27477-0.

55. Yusuf, I., Kageyama, R., Monticelli, L., Johnston, R.J., Ditoro, D., Hansen, K., Barnett, B., and Crotty, S. (2010). Germinal center T follicular helper cell IL-4 production is dependent on signaling lymphocytic activation molecule receptor (CD150). J. Immunol. *185*, 190–202. https://doi.org/10.4049/jimmunol.0903505.

56. Brand, K.A., and Hermfisse, U. (1997). Aerobic glycolysis by proliferating cells: a protective strategy against reactive oxygen species. FASEB J *11*, 388–395. https://doi.org/10.1096/fasebj.11.5.9141507.

57. Vardhana, S.A., Hwee, M.A., Berisa, M., Wells, D.K., Yost, K.E., King, B., Smith, M., Herrera, P.S., Chang, H.Y., Satpathy, A.T., et al. (2020). Impaired mitochondrial oxidative phosphorylation limits the self-renewal of T cells exposed to persistent antigen. Nat. Immunol. *21*, 1022–1033. https://doi.org/10.1038/s41590-020-0725-2.

58. Yano, M., Watanabe, K., Yamamoto, T., Ikeda, K., Senokuchi, T., Lu, M., Kadomatsu, T., Tsukano, H., Ikawa, M., Okabe, M., et al. (2011). Mitochondrial dysfunction and increased reactive oxygen species impair insulin secretion in sphingomyelin synthase 1-null mice. J. Biol. Chem. *286*, 3992–4002. https://doi.org/10.1074/jbc.M110.179176.

59. Lyakhovich, A. (2013). Damaged mitochondria and overproduction of ROS in Fanconi anemia cells. Rare Dis. *1*, e24048. https://doi.org/10.4161/rdis.24048.

60. Brint, E., O'Callaghan, G., and Houston, A. (2013). Life in the Fas lane: differential outcomes of Fas signaling. Cell. Mol. Life Sci. *70*, 4085–4099. https://doi.org/10.1007/s00018-013-1327-z.

61. Yuan, K., Jing, G., Chen, J., Liu, H., Zhang, K., Li, Y., Wu, H., McDonald, J.M., and Chen, Y. (2011). Calmodulin mediates Fas-induced FADD-independent survival signaling in pancreatic cancer cells via activation of Src-extracellular signal-regulated kinase (ERK). J. Biol. Chem. *286*, 24776–24784. https://doi.org/10.1074/jbc.M110.202804.

62. Lavrik, I.N., Golks, A., Riess, D., Bentele, M., Eils, R., and Krammer, P.H. (2007). Analysis of CD95 threshold signaling: triggering of CD95 (FAS/APO-1) at low concentrations primarily results in survival signaling. J. Biol. Chem. *282*, 13664–13671. https://doi.org/10.1074/jbc.M700434200.

63. Freiberg, R.A., Spencer, D.M., Choate, K.A., Duh, H.J., Schreiber, S.L., Crabtree, G.R., and Khavari, P.A. (1997). Fas signal transduction triggers either proliferation or apoptosis in human fibroblasts. J. Invest. Dermatol. *108*, 215–219. https://doi.org/10.1111/1523-1747.ep12334273.

64. Suzuki, I., Martin, S., Boursalian, T.E., Beers, C., and Fink, P.J. (2000). Fas ligand costimulates the in vivo proliferation of CD8+ T cells. J. Immunol. *165*, 5537–5543. https://doi.org/10.4049/jimmunol.165.10.5537.

65. Klebanoff, C.A., Scott, C.D., Leonardi, A.J., Yamamoto, T.N., Cruz, A.C., Ouyang, C., Ramaswamy, M., Roychoudhuri, R., Ji, Y., Eil, R.L., et al. (2016). Memory T cell-driven differentiation of naive cells impairs adoptive immunotherapy. J. Clin. Invest. *126*, 318–334. https://doi.org/10.1172/JCI81217.

66. Lai, Y.J., Lin, V.T.G., Zheng, Y., Benveniste, E.N., and Lin, F.T. (2010). The adaptor protein TRIP6 antagonizes Fas-induced apoptosis but promotes its effect on cell migration. Mol. Cell Biol. *30*, 5582–5596. https://doi.org/10.1128/MCB.00134-10.

67. Guégan, J.P., and Legembre, P. (2018). Nonapoptotic functions of Fas/CD95 in the immune response. FEBS J. *285*, 809–827. https://doi.org/10.1111/febs.14292.

68. Jiang, C., Loo, W.M., Greenley, E.J., Tung, K.S., and Erickson, L.D. (2011). B cell maturation antigen deficiency exacerbates lymphoproliferation and autoimmunity in murine lupus. J. Immunol. *186*, 6136–6147. https://doi.org/10.4049/jimmunol.1001931.

69. Peperzak, V., Vikström, I., Walker, J., Glaser, S.P., LePage, M., Coquery, C.M., Erickson, L.D., Fairfax, K., Mackay, F., Strasser, A., et al. (2013). Mcl-1 is essential for the survival of plasma cells. Nat. Immunol. *14*, 290–297. https://doi.org/10.1038/ni.2527.

70. O'Connor, B.P., Raman, V.S., Erickson, L.D., Cook, W.J., Weaver, L.K., Ahonen, C., Lin, L.L., Mantchev, G.T., Bram, R.J., and Noelle, R.J. (2004). BCMA is essential for the survival of long-lived bone marrow plasma cells. J. Exp. Med. *199*, 91–98. https://doi.org/10.1084/jem.20031330.

71. Pradelli, L.A., Bénéteau, M., Chauvin, C., Jacquin, M.A., Marchetti, S., Muñoz-Pinedo, C., Auberger, P., Pende, M., and Ricci, J.E. (2010). Glycolysis inhibition sensitizes tumor cells to death receptors-induced apoptosis by AMP kinase activation leading to Mcl-1 block in translation. Oncogene *29*, 1641–1652. https://doi.org/10.1038/onc.2009.448.

72. Liu, L., Lu, Y., Martinez, J., Bi, Y., Lian, G., Wang, T., Milasta, S., Wang, J., Yang, M., Liu, G., et al. (2016). Proinflammatory signal suppresses proliferation and shifts macrophage metabolism from Myc-dependent to HIF1alpha-dependent. Proc Natl Acad Sci USA *113*, 1564–1569. https://doi.org/10.1073/pnas.1518000113.

73. Lam, W.Y., Becker, A.M., Kennerly, K.M., Wong, R., Curtis, J.D., Llufrio, E.M., McCommis, K.S., Fahrmann, J., Pizzato, H.A., Nunley, R.M., et al. (2016). Mitochondrial Pyruvate Import Promotes Long-Term Survival of Antibody-Secreting Plasma Cells. Immunity *45*, 60–73. https://doi.org/10.1016/j.immuni.2016.06.011.

74. Hemmi, H., Kaisho, T., Takeuchi, O., Sato, S., Sanjo, H., Hoshino, K., Horiuchi, T., Tomizawa, H., Takeda, K., and Akira, S. (2002). Small anti-viral compounds activate immune cells via the TLR7 MyD88-dependent signaling pathway. Nat. Immunol. *3*, 196–200. https://doi.org/10.1038/ni758.

75. Li, B., and Dewey, C.N. (2011). RSEM: accurate transcript quantification from RNA-Seq data with or without a reference genome. BMC Bioinf. *12*, 323. https://doi.org/10.1186/1471-2105-12-323.

76. Langmead, B., Trapnell, C., Pop, M., and Salzberg, S.L. (2009). Ultrafast and memory-efficient alignment of short DNA sequences to the human genome. Genome Biol. *10*, R25. https://doi.org/10.1186/gb-2009-10-3-r25.

77. Robinson, M.D., McCarthy, D.J., and Smyth, G.K. (2010). edgeR: a Bioconductor package for differential expression analysis of digital gene expression data. Bioinformatics *26*, 139–140. https://doi.org/10.1093/bioinformatics/btp616.

78. Xie, Z., Bailey, A., Kuleshov, M.V., Clarke, D.J.B., Evangelista, J.E., Jenkins, S.L., Lachmann, A., Wojciechowicz, M.L., Kropiwnicki, E., Jagodnik, K.M., et al. (2021). Gene Set Knowledge Discovery with Enrichr. Curr. Protoc. *1*, e90. https://doi.org/10.1002/cpz1.90.

79. Bult, C.J., Blake, J.A., Smith, C.L., Kadin, J.A., and Richardson, J.E.; Mouse Genome Database Group (2019). Mouse Genome Database (MGD) 2019. Nucleic Acids Res. *47*, D801–D806. https://doi.org/10.1093/nar/gky1056.

80. Heng, T.S.P., and Painter, M.W.; Immunological Genome Project Consortium (2008). The Immunological Genome Project: networks of gene expression in immune cells. Nat. Immunol. *9*, 1091–1094. https://doi.org/10.1038/ni1008-1091.

81. Kingsmore, K.M., Bachali, P., Catalina, M.D., Daamen, A.R., Heuer, S.E., Robl, R.D., Grammer, A.C., and Lipsky, P.E. (2021). Altered expression of genes controlling metabolism characterizes the tissue response to immune injury in lupus. Sci. Rep. *11*, 14789. https://doi.org/10.1038/s41598-021-93034-w.

STAR★METHODS

KEY RESOURCES TABLE

REAGENT or RESOURCE	SOURCE	IDENTIFIER
Antibodies		
CD45R/B220 Pacific Blue	BioLegend	RRID:AB_492876
CD11c AF700	BioLegend	RRID:AB_528736
Anti-MU/HU GL7 AF647	BioLegend	RRID:AB_2562185
CD138 PE	BioLegend	RRID:AB_10916119
CD62L PerCP/Cyanine5.5	BioLegend	RRID:AB_2285839
CD95/FAS PE-Cy7	BD Biosciences	RRID:AB_396768
CD185/CXCR5 BV421	BioLegend	RRID:AB_256128
CD44 APC/Cyanine7	BioLegend	RRID:AB_830785
CD279/PD-1 PE/Cyanine7	BioLegend	RRID:AB_572017
CD11b BV650	BioLegend	RRID:AB_2566568
CD45R/B220 BV711	BioLegend	RRID:AB_2563491
CD4 BV650	BioLegend	RRID:AB_2562098
CD45RA PE	BioLegend	RRID:AB_314412
IgD AF488	BioLegend	RRID:AB_11150595
CD4 BV421	BioLegend	RRID:AB_10965645
CD45RO APC/Cyanine7	BioLegend	RRID:AB_10899580
CD20 AF700	BioLegend	RRID:AB_493753
CD268/BR3 PE/Cyanine7	BioLegend	RRID:AB_2565592
CD21/CD35 AF647	BioLegend	RRID:AB_2629578
CD21/CD35 FITC	BioLegend	RRID:AB_940405
CD23 PE	BioLegend	RRID:AB_312833
Glut1 AF488	Abcam	RRID:AB_2714026
IL-21 PE	BioLegend	RRID:AB_1279430
Ki-67 APC	BioLegend	RRID:AB_2561930
IL-6 PE	BioLegend	RRID:AB_315338
CD32/CD16	Leinco	RRID:AB_2829820
CD45 PE/Cyanine7	BioLegend	RRID:AB_2860726
CD4 FITC	BioLegend	RRID:AB_312691
PD-1 PE	BioLegend	RRID:AB_1877231
PD-1 APC	BioLegend	RRID:AB_2159183
PD-1 PD/Cyanine7	BioLegend	RRID:AB_572017
CD25 FITC	BioLegend	RRID:AB_493333
CXCR5 BV421	BioLegend	RRID:AB_2562128
Rat IgG2a	BioLegend	RRID:AB_345338
Rat IgG2b	BioLegend	RRID:AB_492998
CD38 APC/Cyanine7	BioLegend	RRID:AB_2616967
Anti-Mouse CD3 (17A2)	Leinco	RRID:AB_2737469
Anti-Mouse CD28	Leinco	RRID:AB_2828714
PNA-fluorescein	Vector Laboratories	FL-1071-5
IgD-AF594	BioLegend	RRID:AB_2565572

(*Continued on next page*)

Continued

REAGENT or RESOURCE	SOURCE	IDENTIFIER
Bacterial and virus strains		
APRIL CAR-T Retrovirus	This paper	N/A
Empty Vector Retrovirus	This paper	N/A
Chemicals, peptides, and recombinant proteins		
MitoTracker™ Green FM	ThermoFisher	Cat#M46750
BioTracker™ ATP-Red	MilliporeSigma	Cat#SCT045
MitoSOX™	ThermoFisher	Cat#M36008
MitoTracker™ Red FM	ThermoFisher	Cat#M22425
2-NBDG	Glpbio	Cat#GC10289
BD GolgiStop™	BD PharMingen	Cat#554724
PMA	MilliporeSigma	Cat#P1585
Ionomycin	MilliporeSigma	Cat#I9657
Annexin Staining Buffer	In-house Preparation	N/A
NP-Ovalbumin	LGC Biosearch Technology	Cat#N-5051
Alum Adjuvant	FisherScientific	Cat#50-134-4534
2-Deoxy-D-glucose	ThermoFisher	Cat#111980250
UK5099	Glpbio	Cat#GC11865
BPTES	Cayman Chemical	Cat#19284
Thioridazine	Cayman Chemical	Cat#14400
Etomoxir	Cayman Chemical	Cat#11969
FCCP	Sigma	Cat#370-86-5
Rotenone	Sigma	Cat#557368
Antimycin	Sigma	Cat#A8674
Oligomycin	Sigma	Cat#1404-19-9
3-Bromopyruvic Acid	Cayman Chemical	Cat#19068
Poly-D-Lysine Hydrobromide	FisherScientific	Cat#ICN15017510
Scigen Tissue-Plus™ O.C.T. Compound	FisherScientific	Cat#23-730-571
Leica IHC/ISH Super Block	Leica Biosystems	Cat#PV6122
Human IL-2	Peprotech	Cat#200-02
RPMI medium 1640	Life Technologies	Cat#11875-093
Fetal Bovine Serum	Gibco	Cat#SH3091003
Penicillin-Streptomycin Solution	Life Technologies	Cat#15140122
2-Mercaptoethanol	Sigma-Aldrich	Cat#M3148
L-Glutamine	Life Technologies	Cat#25030-081
Dulbecco's Phosphate Buffered Saline (PBS)	Life Technologies	Cat#14190-144
Sodium Chloride	Sigma-Aldrich	Cat#S9888
Calcium Chloride	Sigma-Aldrich	Cat#C4901
HEPES Solution	Sigma-Aldrich	Cat#H3537
DMEM	Life Technologies	Cat#11965118
Seahorse Media	In-house Preparation	N/A
Sodium Pyruvate	Sigma-Aldrich	Cat#P5280
Critical commercial assays		
BD Cytofix/Cytoperm™ Fixation and Permeabilization Solution	BD Biosciences	Cat#554722
FITC Annexin V Apoptosis Detection Kit with PI	BioLegend	Cat#640914

(*Continued on next page*)

Continued

REAGENT or RESOURCE	SOURCE	IDENTIFIER
Seahorse XF Real-Time ATP Rate Assay Kit	Agilent	Cat#103592
Glucose Assay Kit	Eton Bioscience	Cat#1200032002
miRNeasy Mini Extraction Kit	Qiagen	Cat#217084
High-Capacity cDNA Reverse Transcription Kit	Applied Biosystems	Cat#4368814
ProLong™ Diamond Antifade Mountant	Invitrogen	Cat#P36970
Deposited data		
RNAseq Data	This paper	GEO: GSE224148
RNAseq Data	Andreoletti et al.[43]	GEO: GSE164457
Experimental models: Cell lines		
HEK293T	ATCC	Cat#CRL-1573
Experimental models: Organisms/strains		
C57BL/6J	The Jackson Laboratory	Cat#000664
BXSB.Cg-*Cd8a*^{tm1Mak} *Il15*^{tm1Imx}/Dcr *Yaa*	In-house Breeding	N/A
NZBWF1/J	The Jackson Laboratory	Cat#100008
BXSB.B6-*Yaa*$^{+}$/MobJ	The Jackson Laboratory	Cat#001925
Oligonucleotides		
Xbp1 Primer Set	IDT	N/A
Xbp1s Primer Set	IDT	N/A
Actb Primer Set	IDT	N/A
Software and algorithms		
Leica Application Suite X Software	Leica	https://www.leica-microsystems.com/products/microscope-software/p/leica-las-x-ls/
ImageJ	NIH	https://imagej.nih.gov/ij/
Prism	GraphPad	https://www.graphpad.com/features
Hot Bubbleplot Generator	Visual Paradigm	https://online.visual-paradigm.com/charts/explore/bubble-chart-maker/
FlowJo V10	TreeStar	https://www.flowjo.com/
Gene Set Enrichment Analysis (GSEA)	UC San Diego and Broad Institute	https://www.gsea-msigdb.org/gsea/index.jsp
Gene Set Variation Analysis (GSVA)	Bioconductor	https://www.bioconductor.org/packages/release/bioc/html/GSVA.html

RESOURCE AVAILABILITY

Lead contact

Additional information and requests for resources and reagents should be directed to, and will be fulfilled by, the lead contact, Dr. Chih-Hao Chang (lucas.chang@jax.org).

Materials availability

This study did not generate new unique reagents.

Data and code availability

- RNA sequencing data is publicly available through Gene Expression Omnibus (GSE224148).
- This paper does not report original code.
- Any additional information required to reanalyze the data reported in this paper is available from the lead contact upon request.

EXPERIMENTAL MODEL AND SUBJECT DETAILS

Mice and treatments

BXSB.Cg-*Cd8a*^{tm1Mak} *Il15*^{tm1Imx}/Dcr *Yaa* (*Yaa* DKO, JAX#018137), NZBWF1/J (JAX#100008), BXSB.B6-*Yaa*$^{+}$/MobJ (JAX#001925), and C57BL/6J (B6, JAX#000664) mice were bred and housed at The Jackson Laboratory (Bar Harbor, Maine). Mice were provided 10% fat food JL Mouse Breeder/Auto (LabDiet® 5K20) and water *ad libitum*; they were housed on a 14-hour light, 10-hour dark cycle in a specific pathogen-free room. Symptomatic male *Yaa* DKO mice had visibly swollen lymph nodes and displayed elevated cellular disease biomarkers (often found at age 10–12 weeks old); whereas pre-symptomatic males (6–7 weeks old) had yet to develop these manifestations. Female littermate mice lacking the *Yaa*-containing Y chromosome have extremely slow disease progression and initiate a very mild autoimmune reaction that manifests later in life with a reduced pathogenicity and were used as healthy controls.[19] Symptomatic NZBWF1 mice were 36-40-week-old females with elevated cellular disease biomarkers. Before experiments, mice were bled to verify disease state. Experiments were performed on symptomatic mice unless otherwise stated. Mice in survival experiments were euthanized when classified as moribund, and mice euthanized before this point or for non-lupus-related issues were excluded from survival data. For *in vivo* metabolic treatments, 2DG (Thermo Fisher) was dissolved in drinking water (6 g/L) and was provided to mice *ad libitum*. For immunization studies, mice received a single intraperitoneal injection of 50 μg of NP-Ovalbumin in aluminum hydroxide and were euthanized for splenic analysis 14 days later. Animal studies were approved by Institutional Animal Care and Use Committee at The Jackson Laboratory.

METHOD DETAILS

Flow cytometry and intracellular staining

Single-cell suspensions from peripheral blood, spleens, or lymph nodes were blocked with anti-CD16/32 and stained with antibody cocktails on ice after red blood cell lysis. Flow cytometry data was acquired on an LSR II flow cytometer and was analyzed using FlowJo software version 10.6.1. Intracellular staining was performed with the Fixation/Permeabilization Solution Kit (BD Biosciences) in the presence of GolgiStop (BD PharMingen) using manufacturer's recommendations with cells stained overnight on ice. For IL-6 staining, cells were restimulated for 4 hours with 50 ng/ml PMA (Sigma), and 500 ng/ml ionomycin (Sigma). Cell populations were either used directly or further purified by a FACSAria II cell sorter. For apoptosis detection, cells were stained for surface markers as described, followed by 2x washing with Annexin staining buffer (PBS with 10 mM HEPES, 150 mM NaCl and 5 mM $CaCl_2$). Cells were then stained at room temperature for 10 minutes in the dark with FITC-Annexin V/propidium iodide (PI) before flow analysis. For measuring mitochondrial mass, mitochondrial membrane potential, ROS and ATP levels, cells were stained with MitoTracker Green FM, MitoTracker Red, MitoSOX (Life Technologies), and BioTracker ATP-Red (MilliporeSigma), respectively, according to the manufacturer's instructions.

All antibodies were purchased from BioLegend, eBioscience or Miltenyi Biotec. The following markers were used to identify each *ex vivo* population: B220^{+} CD4^{-} (total B cells), B220^{+} CD4^{-} CD138^{-} GL7^{+} (activated B cells), B220^{+} CD4^{-} CD138^{-} GL7^{-} (GL7^{-} B cells), B220^{+} CD4^{-} CD138^{-} GL7^{+} CD95^{+} (GCB cells), B220^{+} CD4^{-} CD138^{-} GL7^{-} CD95^{-} (non-GCB cells), B220^{+} CD4^{-} CD138^{+} GL7^{-} (plasmablasts/plasma cells), B220^{-} CD4^{+} (total CD4 T cells), B220^{-} CD4^{+} CXCR5^{+} PD1^{+} (Tfh cells), B220^{-} CD4^{+} CD62L^{-} CD44^{+} (Teff cells), B220^{-} CD4^{+} CD44^{-} CD62L^{+} (naive T cells), B220^{-} CD4^{+} CXCR5^{+} PD1^{+} BCL6^{+} Foxp3^{+} (Tfr cells), B220^{-} CD4^{+} CD25^{+} Foxp3^{+} (Treg cells), B220^{+} CD4^{-} CD21^{-} CD23^{-} (T1 B cells), B220^{+} CD4^{-} CD21^{+} CD23^{+} (T2 B cells), B220^{+} CD4^{-} CD21^{+} CD23^{-} (MZ B cells), B220^{+} CD4^{-} CD21^{-} CD23^{+} (FO B cells), B220^{+} CD4^{-} T-bet^{+} CD11c^{+} (extrafollicular B cells), and B220^{-} CD4^{-} CD11b^{+} (myeloid cells). The following markers were used to identify each mouse *in vitro* activated cell population: B220^{+} CD4^{-} GL7^{+} (activated B cells), B220^{-} CD4^{+} CD62L^{-} CD44^{+} (activated T/Teff-like cells). The following markers were used to identify each human *in vitro* population: CD4^{-} CD20^{+} IgD^{-} BR3^{+} (GCB-like cells) and CD20^{-} CD4^{+} CD45RA^{-} CD45RO^{+} (activated T/Teff-like cells).

Cell survival assays

Yaa DKO splenocytes or healthy human PBMCs (Precision for Medicine, MD) were cultured at 4x10^{6} per ml of R10 medium (RPMI plus 10% FBS, 2 mM L-glutamine, 50 μM 2-ME, 100 U/ml penicillin, and 100 μg/ml streptomycin) with 0.5 μg/ml of anti-CD3/28 antibodies, 100 U/ml IL-2 and 30 ng/ml of the TLR7 agonist R848 (Adipogen) for 2 days to achieve cellular activation.[74] On day 2, the cells were harvested and plated at 2.5x10^{6} cells per ml in R10 medium with 0, 0.2, or 1 mM 2DG onto a 96-well plate at 200 μl per well. Cells

were stained with antibody cocktail and analyzed by flow cytometry to ascertain numbers of live cells of each type by PI staining. For measuring viability of *ex vivo* cells, splenocytes of symptomatic *Yaa* DKO mice were sorted and plated at $1x10^5$ cells per ml in R10 media with or without indicated glycolysis inhibitors for 1–2 days. Cells were harvested and analyzed by flow cytometry to ascertain live cell numbers.

Metabolic assays

Immune cells were extracted from spleen and lymph nodes of lupus-prone mice and were sorted via FACSAria II in complete cell culture medium. Cells were sorted with a 70 μM nozzle into a tube containing a solution of 50% fetal bovine serum and 50% complete cell culture medium. Cells were counted and dead cells (<5% of the samples) were excluded. Seahorse plates were coated with 20 μl/well of 50 μg/ml poly-d-lysine for 1–2 hours before plating the cells in seahorse medium at 100,000 cells per well, where they were left to acclimate to these conditions for 45 minutes before initiating assays on an Agilent Seahorse XFe96 Analyzer. Oxygen consumption rates (OCR) and extracellular acidification rates (ECAR) were measured in Seahorse XF assay media (non-buffered RPMI 1640 containing 25 mM glucose, 2 mM L-glutamine, and 1 mM sodium pyruvate) under basal conditions and in response to 25 mM 2DG, 20 μM UK5099, 10 μM BPTES, 40 μM etomoxir, or 100 nM thioridazine with the addition of 1 μM oligomycin, 1.5 μM fluorocarbonyl cyanide phenylhydrazone (FCCP), and 100 nM rotenone plus 1 μM antimycin A (Sigma) with a XF-96^e Extracellular Flux Analyzer (Seahorse Bioscience). Cellular rates of ATP production were measured by Seahorse Real-Time ATP Rate kit and calculated according to manufacturer's recommendations. All assays were performed with equal numbers of cells per well in each group. Maximal respiratory capacity (MRC) was assessed as the percentage of baseline OCR after FCCP injection. Glycolytic reserve was calculated as the percent increase over basal ECAR after oligomycin injection. Metabolic dependency was determined by the reduction effect of indicated inhibitors of glycolysis, glutaminolysis, or fatty acid oxidation on MRC as an indicator of cellular reliance on substrates derived from certain oxidative pathways, fueling OXPHOS.[31] The MRC values from treated cells were normalized to those from untreated cells and presented as MRC % of untreated. For analysis of glucose uptake, mice were injected with 50 μg of 2-NBDG via tail vein 20 minutes before spleens were harvested. Cells were stained for surface markers and intensity of 2-NBDG in each population was assessed by flow cytometry. Glucose concentrations were determined using a Glucose Assay Kit (Eton Biosciences), according to manufacturer's specifications and readings were carried out using a SpectraMax i3 spectrophotometer (Molecular Devices) at 490 nm absorbance.

Immunohistochemistry

Six-micron sections were cut from fresh spleen tissue frozen in OCT medium and were mounted on slides, fixed with ice-cold acetone for 15 minutes, and re-hydrated for 10 minutes with PBS. Leica SuperBlock was used to block the slides for 30 minutes before staining with PNA-fluorescein at 20 μg/ml and IgD-AlexaFluor 594 at 5 μg/ml for 1 hour at room temperature in the dark. Slides were washed 3 times with PBS before mounting sections with Prolong™ Diamond Antifade Mountant (Invitrogen) and were imaged within 24 hours of staining on a Leica Thunder imager per manufacturer's recommendations. Individual images were merged using the 'mosaic merge' function in Leica Application Suite X software and were exported into Fiji for image analysis. GCs were identified as areas of PNA staining surrounded by IgD-stained cells. GC size was calculated by measuring the area of PNA stain within each GC three times and taking the average of these replicates for the final area.

Gene expression analysis by RNA-sequencing and quantitative real-time PCR

RNA-sequencing (RNA-seq) was performed by The Jackson Laboratory Genome Technologies Scientific Service. Total RNA of spleens (4 samples per group) was isolated with the QIAGEN miRNeasy mini extraction kit (QIAGEN) and cDNA was synthesized with the High-Capacity cDNA Reverse Transcription Kit (Applied Biosystems). RNA quality was assessed with a Bioanalyzer 2100 (Agilent Technologies). Poly(A)-selected RNA-seq libraries were generated using the Illumina TruSeq RNA Sample preparation kit v2. RNA-seq was performed in a 75-bp paired-end format with a minimum of 40 million reads per sample on the Illumina NextSeq 500 platform according to the manufacturer's instructions. RNA-seq reads were filtered and trimmed for quality scores >30 using a custom python script. The filtered reads were aligned to *Mus musculus* GRCm38 using RSEM (v1.2.12)[75] with Bowtie2 (v2.2.0)[76] (command: rsem-calculate-expression -p 12 –phred33-quals –seed-length 25 –forward-prob 0 –time –output-genome-bam – bowtie2). RSEM calculates expected counts and transcript per million (TPM). The expected counts from RSEM were used in the Bioconductor edgeR 3.20.9 package[77] to determine differentially expressed genes.

Principle component analysis (PCA) was performed using the plotPCA() function of the R/Bioconductor package DESeq2 (v 1.28.1). The volcano plot and heatmap of DEGs were produced using the R package ggplots (v 3.3.1). KEGG pathway and GO term enrichment of DEGs up- and down-regulated with 2DG treatment was calculated using Enrichr.[78] Bubbleplots of Enrichr results were generated using a "Hot Bubbleplot Generator" online java application built using the D3 (Data-Driven Design) and ReactJS javascript libraries. Determination of the most significantly different gene groups was performed with Gene Set Enrichment Analysis (GSEA).[24,25] The following gene sets from the Molecular Signatures Database were used: systematic names, M12175 (Systemic Lupus Erythematosus) and M12930 (Immunoglobin Production). Groups were deemed significant at an FDR *q*-value of 0.05 or below. Genes of interest for each group were extracted based on the core enrichment value provided by GSEA. Quantitative real-time PCR (qPCR) was performed by the SYBR green method, with an Applied Biosystems ViiA 7 Real-Time PCR System (Life Technologies). Quantitation of the results was performed by the comparative Ct (2-[delta][delta]Ct) method. The Ct value for each sample was normalized to the value for beta-actin. The sequences of qPCR primers are listed in Table S1. All RNAseq data have been uploaded to Gene Expression Omnibus and are available under accession number GSE224148.

Gene set variation analysis (GSVA)

The R/Bioconductor software package GSVA[26,27] (v1.25.0) was used as a non-parametric, unsupervised method to estimate enrichment of pre-defined gene sets in RNA-seq data from *Yaa* DKO mice. The inputs for GSVA were a matrix of log2 gene expression values for all samples and curated gene sets describing select immune cell types and pathways. Low-intensity probes were filtered out if the interquartile range (IQR) of their log2 expression values across all samples was not greater than zero. Enrichment scores were calculated using a Kolgomorov Smirnoff (KS)-like random walk statistic and represented the greatest deviation from zero for a particular sample and gene set. Scores across all samples were normalized to values between -1 (indicating no enrichment) and +1 (indicating enrichment). Significant differences in enrichment between 6-week, 10-week, and 10-week+2DG cohorts were calculated using Brown-Forsythe and Welch ANOVA tests with Dunnett T3 test for multiple comparisons with an alpha level of 0.05.

GSVA gene set generation and co-expression analysis

Mouse gene sets used as input for GSVA are listed in Tables S2 and S3. Immune-cell and functional-pathway gene signatures were generated by an iterative process involving derivation through literature mining, gene ontology (GO) term definitions provided by the Mouse Genome Informatics (MGI) GO Browser,[79] and immune-cell expression as determined by the Immunological Genome Project Consortium (ImmGen),[80] followed by dataset-specific curation by co-expression analysis. The following GO terms were used to generate the Activated B Cell, Pentose Phosphate Pathway, and Glutamine Metabolism gene sets: GO:0002312-B cell activation involved in immune response, GO:0006098-Pentose phosphate shunt, and GO:0006541 glutamine metabolic process. The glycolysis, oxidative phosphorylation, TCA cycle, and fatty acid oxidation gene signatures have been previously described.[81] The specific gene signatures used in the analysis can be found in Tables S2–S5. The B cell, plasma cell, T cell, activated/effector T cell, Tfh cell, and myeloid cell signatures were derived from Mouse CellScan, a tool for the identification of cellular origin of mouse gene expression datasets. For human data, gene expression analysis was performed on publicly available transcriptomic data (GEO accession: GSE164457)[43] from participants recruited from the California Lupus Epidemiology Study. Briefly, PBMCs were isolated from 120 lupus patients, and were sorted into populations of $CD19^+$ B cells and $CD4^+$ T cells for bulk RNA-seq. GSVA was performed using human orthologs of mouse gene sets listed in Tables S4 and S5. Linear regression analysis between GSVA enrichment scores for activated B cell, activated/effector T cell, total B cell, total T cell, Tfh cell and metabolic pathway gene signatures was carried out as previously described for the mouse RNA-seq data. Co-expression analysis for all gene sets was completed in R using the cor() function to compute Pearson correlation coefficients for log2 expression values of each gene in a given gene set. Gene sets were then refined to maximize the number of co-expressed genes while maintaining specificity for a given cell type or functional pathway. Linear regression analysis between GSVA enrichment scores for immune cell and functional pathway gene signatures was determined using GraphPad Prism software (v9.0.1). For each analysis, the goodness of fit is displayed as the R^2 value. The significance of the slope of the regression line is displayed as the p value.

Retrovirus vector designs and generation of APRIL-based CAR-T cells

The cDNA sequence of the extracellular region of mouse APRIL (nucleotides 319–721, GenBank: Q9D777) was fused to the transmembrane/intracellular domain of CD28 (nucleotides 543–740, GenBank: NM_007642.4) and intracellular domain of CD3ζ (nucleotides 302–643, GenBank: NM_001113391.2) via the hinge of mouse IgG1 and custom-synthesized by Integrated DNA Technologies. The synthesized cDNA was cloned in-frame into the MSCV-IRES-GFP-based retroviral vector.[16] For generating retroviruses, APRIL or empty control vectors were transfected into 293T cells, together with helper plasmid, and the resulting culture viral supernatants were used to transduce $CD8^+$ T cells isolated from BXSB.B6-*Yaa*$^+$ mice, a BXSB-consomic strain that does not carry the *Yaa* mutation and does not develop lupus-like disease. Cells were activated with 0.5 μg/ml of anti-CD3/28 antibodies and 100 U/ml IL-2 for 1 day and exposed to viral supernatant for 90 minutes (at 2,500 rpm, 30°C) in medium containing hexadimethrine bromide (8 μg/mL), HEPES (1 mM), and IL-2 (100 U/mL). Cells were cultured for an additional 2 days before sorting for GFP-expressing cells, the marker for retroviral expression.

Adoptive transfer

For adoptive transfer of activated B and GCB cells, symptomatic *Yaa* DKO mice were pre-treated with 2DG for one week and were then removed from treatment. Two days after 2DG removal, each mouse was injected intravenously with 1.5 $x10^6$ $GL7^+$ or $GL7^-$ $B220^+$ B cells sorted from untreated, symptomatic *Yaa* DKO mice. For adoptive transfer of APRIL-based CAR-T cells, $1x10^6$ transduced T cells were injected intravenously into symptomatic *Yaa* DKO mice.

QUANTIFICATION AND STATISTICAL ANALYSIS

Statistical analysis

Comparisons for two groups were calculated by using an unpaired, two-tailed Student's *t* test. Comparisons for more than two groups were calculated using a one-way ANOVA followed by Bonferroni's multiple comparison tests. Kaplan-Meier curve with Log-rank (Mantel-Cox) test was used for comparisons of survival curves. GSVA analysis comparisons were calculated using Brown Forsythe and Welch's ANOVA followed by Dunnett's T3 multiple comparisons test. All statistical tests were conducted in GraphPad Prism V8.0.2.